IADC-12-09
April 2013

Inter-Agency Space Debris Coordination Committee

International 2008 Optical Debris Campaign

in

Higher Earth Orbit

IADC Action Item 23.4

Working Group 1

ABSTRACT

In the framework of IADC WG1 activities an action item addressed to observation of objects in higher orbit has been issued (AI23.4). The present report contains the description of the joint international observation campaign performed by IADC delegations in the period between February and June 2008. This has been the largest joint observation campaign carried out by the members of Working Group since all delegations participated. Nine space agencies carried out measurements and at least thirteen telescopes were involved in the AI. The whole campaign was spread on a timespan of five new moon weeks starting from February 2008. The observation plan and observation strategies are given in the present report.

A large effort was addressed by the coordinators to prepare a common data exchange form, absolutely mandatory considering the huge amount of data, collected by different partners, to be analysed. The used form is described in the report.

The AI main objective is the comparison of data achieved with the data collected in 2004 during the joint international observation campaign related to IADC AI21.2 in order to evaluate differences or similiarities to better understand the space debris HEO population evolution. A brief analysis of collected data is given in the present report.

TABLE OF CONTENTS

List of abbreviations

AIUB	Astronomical Institute of the University of Bern
ASI	Italian Space Agency
BSGC	Bisei Spaceguard Center
CCD	Charge Coupled Device
CNES	Centre National d'Etudes Spatiales
ESA	European Space Agency
ESASDT	ESA Space Debris Telescope
FOV	Field Of View
GEO	Geostationary Earth Orbit
GEODSS	Ground-Based Electro-Optical Deep Space Surveillance
GTO	Geosynchronous Transfer Orbit
IADC	Inter-Agency Space Debris Coordination Committee
JAXA	Japan Aerospace Exploration Agency
LEO	Low Earth Orbit
MEO	Medium Earth Orbit
MODEST	Michigan Orbital Debris Survey Telescope
NASA	National Aeronautics and Space Administration
OGS	Optical Ground Station (ESA 1-m telescope, Tenerife)
SpaDe	Italian Space Debris Observatory
TAROT	Telescope a Action Rapide pour les Objets Transitoires
TLE	Two Line Elements
UKSA	United Kingdom Space Agency
USSTRATCOM	United States Strategic Command

Report structure

The report is organized in the sequent subsections

- Description of campaign
- Description of observation plan
- Discussion on results
- Appendices

The first part, related to the general description of the observation campaign, includes objectives and background of the action item AI23.4. In the same section a general overview of the campaign is given, all participants delegations are treated as a whole in this section highlighting the broad dimension of the group of participants as well as its worldwide spreading.

In the second section the description of the observation plan is detailed, including observing technique and strategies and the analytic list of observed fields.

Last section of the reports includes a discussion of the results, the magnitude and orbital parameter distribution is given. Statistics on correlated and uncorrelated target are given and comparison with respect to the previous observation campaign in HEO (AI21.2) is given

Appendices includes single participants contributions: a description for each participating sensor (sensor description form) , survey procedures, list of the planned and eventually acquired observations ,

History of IADC HEO observation campaigns

- **12.1 – 1997-1998: ESA, NASA**
- **18.1 – Jan – Mar 2002: ESA, NASA**
- **20.2 – Oct 2002 – Mar 2003: ESA, NASA, ASI, JAPAN, BNSC**
- **21.2 – Jan – Sept 2004: BNSC, CNES, ESA, JAXA, NASA**

The AI23.4 observation campaign

At the 23th Inter-Agency Space Debris Coordination Committee (IADC) Meeting was decided to perform a new international observation campaign for debris in higher orbit with the aim to compare and if required complete the results achieved during the previous one (AI 21.2 , International Optical Debris campaign in Higher Orbit). Objectives of this campaign were to determine the extent and character of debris in HEO, specifically by obtaining distributions for the brightness, inclination, right ascension of ascending node, and mean motion for the debris. Where possible, complete sets of orbital parameters were calculated in order to discriminate GEO objects from ones in different orbits (e.g., GTO). Moreover the orbital analysis of UCT objects permitted avoiding an overestimation of the number of GEO objects by eliminating repeated counts of the same object. This observation campaign was a further step in the development of an understanding of the space debris situation in HEO through the following points:

- Continue statistical monitoring of 8+ hour period orbital regimes.
- Initiate small-object optimized observations of clusters in orbit pole distribution to provide information on evolution of GEO break-ups.
- Seek advice from WG2 to optimize search strategies for small objects.
- Facilitate opportunities for inter-facility co-operation by defining simple formats for exchange of data as appropriate.
- Initiate collaborative observing of found objects with significant night-to-night motion, such as GTO and librating/drifting GEO debris.
- Extend observing techniques to enable estimation of eccentricity to minimize contamination of surveys by e>0 objects.
- Ensure inclusion of groups with different experience within campaign.

Observational surveys were carried out by delegations of all nations participating in WG1. These surveys took the form of a common, coordinated observation campaign based on a common plan. Participating delegations were ASI, CNES, CNSA, ESA, JAXA, NASA, NSAU, ROSCOSMOS, BNSC.

Shown below are the sensors involved in AI23.4 observation campaign spreading all around the world:

The nine delegations who reported observing and their sites:

1. ASI
2. CNES
3. CNSA
4. ESA
5. JAXA
6. NASA
7. NSAU
8. ROSCOSMOS
9. UKSA

The Aperture versus the field of view of the involved sensors are shown in the following.

Aperture [mm]	FOV [°]
300	2,6 ASI
250	0,73 ASI
400	0,6 BNSC
250	1,86 CNES
1040	2 CNSA
1000	0,66 ESA
1000	2 JAXA
350	1,26 JAXA
610	1,3 NASA
410	0,33 NASA
220	2,8 ROS
640	1 ROS
2600	0,14 ROS

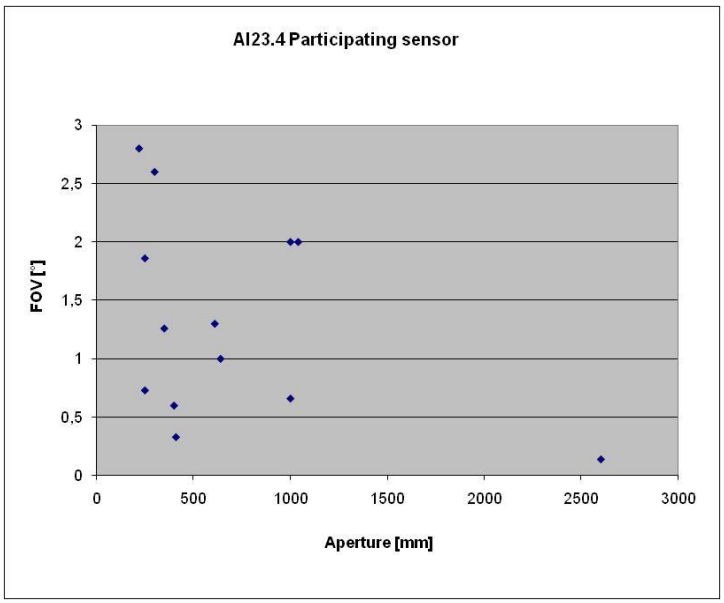

Results

Final reports were received from the following seven delegations:

1. ASI
2. CNES
3. CNSA
4. ESA
5. JAXA
6. NASA
7. UKSA.

The reports are attached to this document.

Conclusions

All of the delegations reported similar results as previous years: a distribution of bright objects near V = 12th magnitude, which for cataloged objects, are primarily intact spacecraft and rocket bodies. Where telescope size allowed going fainter, a second distribtion of fainter, largely uncataloged objects, was found fainter than 15th magnitude. The assumption is that this fainter distribution is largely debris.

No large scale differences were noted between the various delegations this year, and results from previous years. Unfortunately, it proved impossible to normalize the various reports onto one, standard summary plot.

Appendices

Adopted WG1 AI23.4

Inter-Agency Space Debris Coordination Committee

30 March 2005

Action item:	Title:	Assignment
23.4	INTERNATIONAL 2007 OPTICAL DEBRIS CAMPAIGN IN HIGHER EARTH ORBIT	WG1

Description:

Objectives:

* continue statistical monitoring of 8+ hour period orbital regimes

* initiate small-object optimised observations of clusters in orbit pole distribution, as seen in previous campaigns, to provide information on evolution of GEO break-ups which is requested by WG2

* seek advice from WG2 to optimize search strategies for small objects

* facilitate opportunities for inter-facility co-operation by defining simple formats for exchange of data as appropriate

* initiate collaborative observing of found objects with significant night-to-night motion, such as GTO and librating/drifting GEO debris

* extend observing techniques to enable estimation of eccentricity to minimise contamination of surveys by e>0 objects for which a circular orbit assumption has been made

* ensure inclusion of groups with different experience within campaign

This action item is an international observing campaign of four one-week windows in duration and its work continues that of current campaigns. The scope includes specific debris clouds near GEO which have been previously identified. The campaign timing will be organized to include consideration of sky, Moon, and site-related constrains as well as group experience.

The data exported by the campaign will be reduced to distribution in the formats agreed between WG1 and WG2, similar in type and scope to previous campaigns.

Opening date:		Closure date:
April 2005		March 2008
Report reference:	**Access:** restricted	

IADC WG1 AI23.4 Observing Plan for Optical Debris observations

IADC WG1 AI 23.4 Observing Plan for Optical Debris Observations

Patrick Seitzer

NASA Delegation

pseitzer@umich.edu

Fabrizio Piergentili

ASI Delegation

Fabrizio.piergentili@uniroma1.it

Version 1.5

In this document we describe the observing dates and observing plans in support of IADC WG1 Action Item 23.4: International 2008 Optical Debris Campaign in Higher Earth Orbit. The goal of this action item is statistical studies of the debris population both at GEO and in the navigation satellite orbits with mean motions near 2 revs/day.

1. Observing Windows

The AI calls for four one-week windows. For runs centered on new moon, suggested starting dates are:

- 5 February 2008 0h UT
- 4 March 2008 0h UT
- 2 April 2008 0h UT
- 1 May 2008 0h UT
- 30 May 2008 0h UT

All of these dates have reasonable galactic latitudes of the right-ascension of the geocentric anti-solar point. For a run starting in the beginning of July, however, the anti-solar point is right in the galactic plane, and source confusion is very strong. Observing debris objects against such a high background of streaked stars is effective only for the very brightest objects. Therefore we recommend that all observations be completed before July 2008.

If at all possible, we recommend that all observatories observe GEO objects during the March and April windows for a coordinated worldwide campaign. Observatories should feel free to observe at times of their own choosing for the two additional weeks.

2. Observing Techniques

The observing techniques to be used are consistent with previous IADC optical campaigns. This will permit comparison of the data obtained in this campaign with data from previous campaigns.

Previous IADC GEO campaigns observed a section of sky close to the anti-solar point (but out of eclipse) for maximum reflected brightness. The next night the telescope is offset by 1.2 degrees in declination (dec), and the observations are repeated at the same right ascension (ra). For the 2008 observing runs, since the Sun is moving North in declination, the anti-solar point is moving south, and so the nightly declination offsets are towards the south to keep as close to the anti-solar point as possible.

If your field of view (fov) is less than 1.2 degrees, then please offset at the same 1.2 degree amount. Your observations will cover the same range of inclination (for circular orbits), but will not be as complete. If your fov > 1.5 degrees, please contact us and we will suggest some alternative pointings.

The faintest objects can be detected if the telescope tracks at the same rate as the object so that the object is detected as a point source, with most of its flux in the smallest number of pixels, and not as a streak. Stars will appear as streaks in these observations.

However, not all GEO objects travel at the same rate and thus some objects will appear as short streaks. In order to keep streak losses low, the exposure times are kept short (typically a few seconds).

Thus for GEO observations there are three possible observing modes: all satisfactory for the goals of this campaign:

1. Point the telescope at the desired *topocentric* ra and dec

a. Turn all drives off.
b. Take N short exposures, where N is at least 10.
c. At the end of the observing sequence, reposition the telescope to the original ra and dec, and start this sequence again.

2. Point the telescope to the specified *topocentric* ra and dec

a. Turn the drive off.
b. Take a single exposure.
c. Reset the telescope to the first ra and dec.
d. Repeat the process for the time period of the observations. This will track a fixed *topocentric* ra and dec: GEO objects will drift in one side and out the other side. How many detections of an individual object one gets depends on your field of view, exposure time, and CCD readout time.
e. If your CCD can drift scan (TDI) like MODEST, then leave the telescope tracking a fixed topocentric ra and dec, and drift scan backwards during the exposure. Stars will appear as streaks, GEO objects as point sources or very short streaks.

3. Point the telescope to the specified *geocentric* ra and dec.

a. Turn drive off.
b. Take a single exposure.
c. Reset the telescope to the first *geocentric* ra and dec, and repeat the procedure for the time period of the observations. In this technique as well objects will drift in one side and out the other side of the field of view.

Note that methods 1) and 2) observe at a fixed *topocentric* ra and dec but each field has a slightly different *geocentric* ra and dec due to the changing parallax between the observatory and the geocenter. But method 3) has a fixed *geocentric* ra and dec but each field has a different *topocentric* ra and dec. Methods 1) and 2) are the easiest to implement on a conventional astronomical telescope.

Please choose the one technique for all of your observations which will give you the greatest probability of success. Do not change methods during the night, or from night to night. Each method samples the orbit

distribution of debris in a different way, and we need each station to be consistent in order for a reasonable analysis.

The above observing methods work for GEO objects. For navigation satellite orbits, however, the rates are much greater. To observe a piece of debris in the GPS orbits, for example, requires tracking under computer control at changing rates. We are most welcome to hear ideas on how to effectively sample this region. One idea is to track using a TLE, and offset the telescope at regular intervals either cross-track or along-track.

Filters – the purpose of this campaign is to go as faint as possible, and not to do colors. Therefore one should observe in as broad a filter as possible, or even open without a filter. Use of narrower filters such as V or R is discouraged. Since we are observing objects reflecting the solar spectrum, one should observe through a filter near the peak of the solar spectrum.

4. Calibration of Observations

Calibration – please calibrate your observations using standard astronomical techniques by observations of standard stars. We recommend at a minimum observing once per photometric night a Landolt (Astronomical Journal, 1992, **88,** page 340) equatorial standard star field with sidereal tracking on for flux calibration. Additional observations may be necessary to determine the extinction.

We also request that each observatory perform once on a photometric night a special series of observations on a Landolt field near the meridian. The exposure time on this field should be the same as the exposure time used for debris observations, in the same filter as debris observations, and N exposures be obtained (N ~ 8). This will permit each observatory to estimate from the standard star observations the sigma of the observed magnitude versus observed magnitude. Observations of debris can not be used to obtain this curve because of tumbling of debris objects. This will also determine accurately the brightness at which the system saturates.

5. Field Positions

For the following fields there will be two fields per night, specified in terms of the geocentric ra and dec. The first field leads earth shadow, the second field trails Earth shadow. At the given local sidereal time, please goto the second field.

In the following tables, all positions are **epoch of date** and **geocentric**. You will need to correct to topocentric depending on your observatory's position. If additional observing time is available, then continue the sequence in steps of 1.2 degrees in declination.

We also show a plot for each month where the fields are with respect to the Earth shadow, and cataloged objects for the middle of the run.

If your fov is < 1.2 degrees, please offset at 1.2-deg step from night to night.

If your field of view is wider than 1.8 degrees, or you have the capability of observing multiple declinations on the same night, then choose geocentric declinations such that:

1. your overlap from night to night is 10%.
2. your geocentric declination in the center of each run is the same as listed for each month.

Thus you will observe more of a range in declination, extending above and below the above fields.

a. February 2008

Change fields at 09h20m local sidereal time.

UT Date	RA (Field 1)	RA (Field 2)	Declination
5 Feb	08h20m	10h20m	14.40 deg
6 Feb	08h20m	10h20m	13.20 deg
7 Feb	08h20m	10h20m	12.00 deg
8 Feb	08h20m	10h20m	10.80 deg
9 Feb	08h20m	10h20m	9.60 deg
10 Feb	08h20m	10h20m	8.40 deg

11 Feb	08h20m	10h20m	7.20 deg

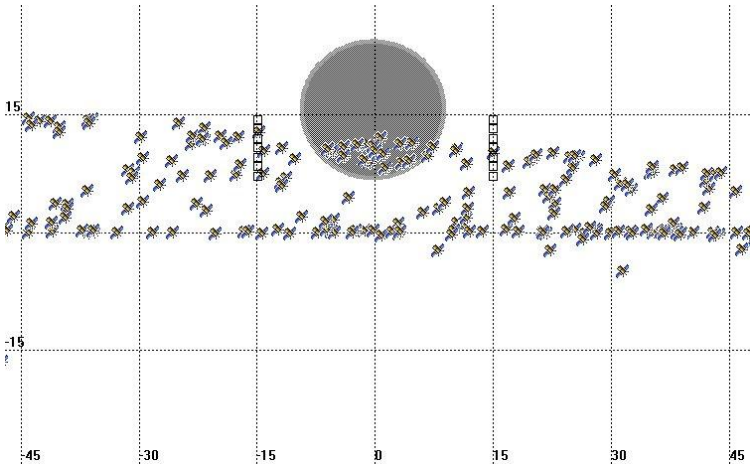

b. March 2008

Change fields at 11h14m local sidereal time.

UT Date	RA (Field 1)	RA (Field 2)	Declination
4 Mar	10h14m	12h14m	8.40 deg
5 Mar	10h14m	12h14m	7.20 deg
6 Mar	10h14m	12h14m	6.00 deg
7 Mar	10h14m	12h14m	4.80 deg
8 Mar	10h14m	12h14m	3.60 deg
9 Mar	10h14m	12h14m	2.40 deg
10 Mar	10h14m	12h14m	1.20 deg

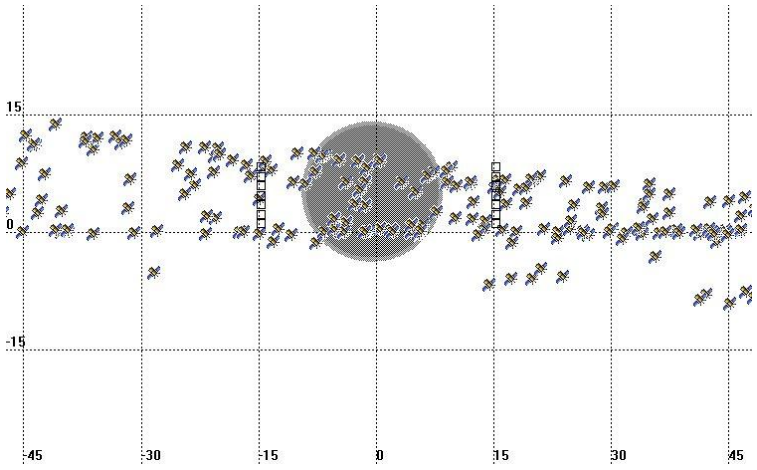
15
0
-15
-45
-30
-15
0
15
30
45

c. April 2008

Change fields at 13h02m local sidereal time.

UT Date	RA (Field 1)	RA (Field 2)	Declination
2 April	12h02m	14h02m	3.60 deg
3 April	12h02m	14h02m	2.40 deg
4 April	12h02m	14h02m	1.20 deg
5 April	12h02m	14h02m	-1.20 deg
6 April	12h02m	14h02m	-2.40 deg
7 April	12h02m	14h02m	-3.60 deg
8 April	12h02m	14h02m	-4.80 deg

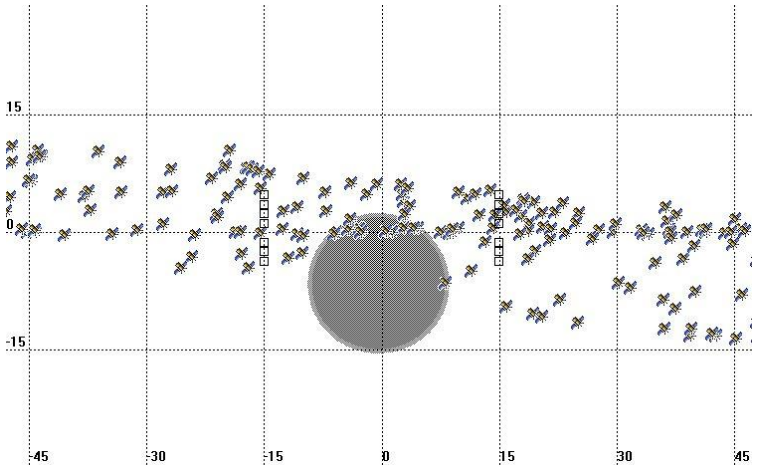

d. May 2008

Change fields at 14h52m local sidereal time.

UT Date	RA (Field 1)	RA (Field 2)	Declination
1 May	13h52m	15h52m	0.0 deg
2 May	13h52m	15h52m	-1.2 deg
3 May	13h52m	15h52m	-2.4 deg
4 May	13h52m	15h52m	-3.6 deg
5 May	13h52m	15h52m	-4.8 deg
6 May	13h52m	15h52m	-6.0 deg
7 May	13h52m	15h52m	-7.2 deg

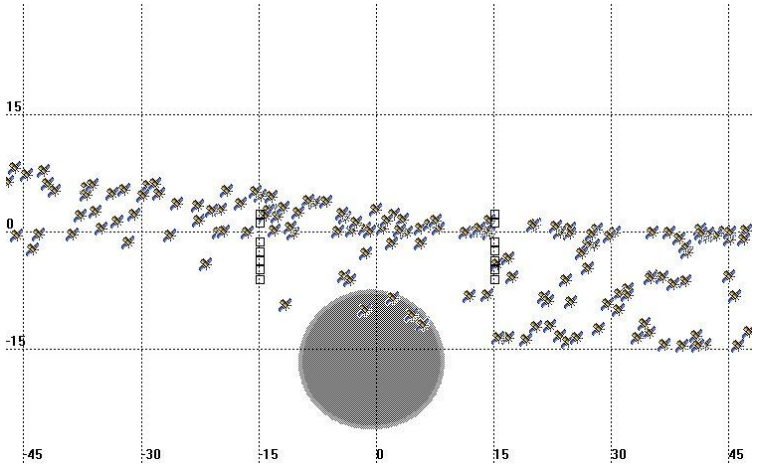

e. June 2008

Change fields at 16h45m local sidereal time. All positions are geocentric.

UT Date	RA (Field 1)	RA (Field 2)	Declination
30 May	15h45m	17h45m	-8.4 deg
31 May	15h45m	17h45m	-9.6 deg

1 June	15h45m	17h45m	-10.8 deg
2 June	15h45m	17h45m	-12.0 deg
3 June	15h45m	17h45m	-13.2 deg
4 June	15h45m	17h45m	-14.4 deg
5 June	15h45m	17h45m	-15.6 deg

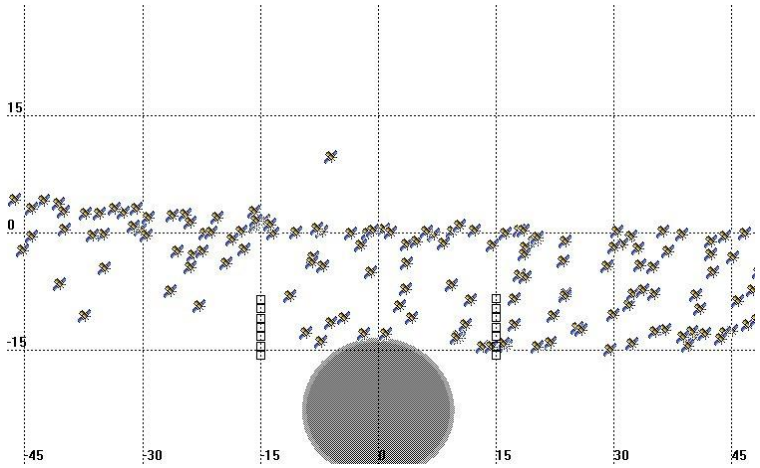

For June, the recommended fields are all very far south, and may be too far south for some northern hemisphere stations to observe effectively. In this case, try the following geocentric fields:

UT Date	**RA (Field 1)**	**RA (Field 2)**	**Declination**
30 May	15h45m	17h45m	0.0 deg
31 May	15h45m	17h45m	-1.2 deg
1 June	15h45m	17h45m	-2.4 deg
2 June	15h45m	17h45m	-3.6 deg
3 June	15h45m	17h45m	-4.8 deg
4 June	15h45m	17h45m	-6.0 deg
5 June	15h45m	17h45m	-7.2 deg

f. Comments

Please send both of us a nightly report of your observations: what the sky conditions were, how many hours you observed, and how many images you obtained.

We will update this document as required. Please send all communications to both of us, in order that one of us gets your email. We will confirm all communications.

Format of delegation report

AI 23.4

International 2008 Optical Debris Campaign

In Higher Earth Orbit

Format of Delegation Reports

Prepared by:

Patrick Seitzer (pseitzer@umich.edu)

and

Fabrizio Piergentili (Fabrizio.piergentili@unibo.it)

This document outlines the format of the report of each delegation who participated in IADC WG1 AI 23.4.

The organizers request that each delegation send two things:

1. a short written report with:
    a. Description of the telescopes and facilities used.
    b. The observing method used.
    c. Data reduction methods
    d. Calibration techniques.
    e. A summary of what your delegation's results are. For example, this could include histograms of magnitudes of detected objects, discussion of selection effects and incompleteness, etc.
2. the data from your delegation:
    a. object data (this is the most important).
    b. fields observed.

c. Tracklets.

The format of the data is given in Appendix 1.

We know that each delegation may not be able to provide all the data requested, but please provide what you can.

Please send your information via email to both of us. We will confirm receiving all emails.

Appendix 1

Data Exchange Format

The Data Exchange form is an excel file, divided in three sheets: object data, fields, and tracklets. Here are the explanations of the different fields to be filled by each delegation.

The most important data to be sent is the object data, followed by the fields, and then the tracklets.

If you can send only one thing, please send as much of the object data as possible. If you can not send in Excel format, then please send in csv or another simple text format.

AI23.4 Data Exchange form, sheet 1: Object

This sheet is intended to collect information on observed objects. The orbital parameters should be determined from your data, not values from the catalog.

Sensor ID: is the name of the observatory

Calibrated Magnitude: is the object mean magnitude calibrated for atmosphere extinction and instrumental zeropoint.

Magnitude error: total error in the calibrated magnitude.

Magnitude System: what filter (BVRI or open) are these observations referred to.

Hour Angle rate: is the object mean hour angle rate expressed in arc-sec/sec

Declination rate: is the object mean declination rate expressed in arc-sec/sec

Corrected Magnitude: is the calibrated magnitude corrected for 42000 km distance and 0 degree phase angle

RAAN: Right Ascension of ascending node, assuming null eccentricity hypothesis if it is not possible to assess complete orbital determination

Inclination: Orbit inclination assuming null eccentricity hypothesis if it is not possible to assess complete orbital determination

Mean Motion: Mean motion evaluated assuming null eccentricity hypothesis if it is not possible to assess complete orbital determination

Eccentricity: include if you were able to do a complete orbital determination. Leave blank if assuming e=0.

UCT/CT(SSN Number): results of comparison with TLE catalogue, the object will be Uncorrelated Target (UCT) or Correlated Target (CT, in this case the SSN number is optional.) Leave this column blank if you did not correlate with the catalog.

AI23.4 Data Exchange form, sheet 2: Fields

This sheet is intended to collect information on observed fields,

Sensor ID: is the name of the observatory

Start Observing time: is the time expressed in year, day of the year, hours, minutes, seconds in which a certain field has been observed.

End Observing time: is the measurement time expressed in year, day of the year, hours, minutes, seconds in which a certain field has been observed

n. of frames: number of frames taken of the considered field of view

RA field center: Geocentric Right Ascension of the considered field of view in degree (assuming 42000 km of distance))

DEC field center: Geocentric Declination of the considered field of view in degree (assuming 42000 km of distance))

Epoch: Epoch of the observation, suggested J2000

AI23.4 Data Exchange form, sheet 3: Tracklets

This sheet is intended to collect all measurements, assembled, by tracklets

Sensor ID: is the name of the observatory

Tracklet ID: is a progressive number starting from 1 assigned to each observed tracklet

Measurement number for this ID: is the number of measurement within the same tracklet (this is a progressive number starting from 1 up to the number of measurements included in the same tracklet)

Time: is the measurement time expressed in year, day of the year, hours, minutes, seconds

Right ascension: the measured geocentric right ascension in degree (assuming 42000 km of distance))

Right ascension error: is the right ascension measurement error in degree

Declination: the measured geocentric declination in degree (assuming 42000 km of distance)

Declination error: is the declination measurement error in degree

Epoch: is the measurement Epoch, possibly J2000

Calibrated Magnitude: is the measurement magnitude calibrated for atmosphere extinction and instrumental zeropoint.

Magnitude error: is the magnitude error.

Reports of Each Delegation

ASI

ASI report on optical observations for IADC AI23.4

Fabrizio Piergentili

Assistant Professor, DIEM, University of Bologna “Alma Mater Studiorum”, Forlì, Italy

fabrizio.piergentili@unibo.it

Maria Libera Battagliere

Scuola di Ingegneria Aerospaziale, “Sapienza” Università di Roma, Rome, Italy

battagliere@gmail.com

Chantal Cappelletti

Scuola di Ingegneria Aerospaziale, “Sapienza” Università di Roma, Rome, Italy

chantal.cappelletti@gmail.com

Fabrizio Paolillo

Scuola di Ingegneria Aerospaziale, “Sapienza” Università di Roma, Rome, Italy

pfabrizio@fastwebnet.it

Manfredi Porfilio

PhD, Agenzia Spaziale Italiana, Rome, Italy

manfredi_porfilio@hotmail.com

Filippo Graziani

Dean of Scuola di Ingegneria Aerospaziale, “Sapienza” Università di Roma, Rome, Italy

filippo.graziani@uniroma1.it

1. Introduction

This document summarizes observations and results obtained by SPADE obserbatory in March 2008 in the framework of IADC WG1 AI23.4 “International 2008 Optical Debris Campaign in Higher Earth Orbit). The goal of this action item is statistical studies of the debris population both at GEO and in the navigation satellite orbits with mean motions near 2 revs/day. All of the work reported here was supported by Italian Space Agency and Group of Astrodynamics of University of Rome “La Sapienza”.

2. Description of instruments and observational techniques

1-INTRODUCTION

Since a few years, the Group of Astrody-namics of the University of Rome “La Sapienza” (GAUSS, Gruppo di Astrodinamica dell’Università degli Studi di Roma “La Sapienza”) has started space debris optical observations in GEO and Low Earth Orbit (LEO). The first observations campaigns were carried out exploiting the facilities of the Associazione Astronomica Frusinate (Frosinone Astronomical Society) which operates the Campo Catino and the Collepardo observatories. Moreover, a joint campaign from Collepardo Automatic Telescope and Observatori Astronòmic de Mallorca (Spain) was performed.

In 2007, in the frame of a contract with the Italian Space Agency (Agenzia Spaziale Italiana, ASI) GAUSS was committed to construct the first Italian observatory completely addressed to space debris monitoring.

The whole observatory design and development has been accomplished involving GAUSS students, facing real problems in structural and optical design.

The features of an optical observatory depend on its purpose. As the observatory is addressed to space debris monitoring, the following requirements were taken into account:

- High brightness for detecting small objects;
- Small focal length, hence large Field of View (FOV) for surveying large regions of space;

- A large Charge Coupled Device (CCD) sensor, hence a large FOV for surveying large regions of space;
- High optical accuracy for orbit determination;
- A mount/workstation/software package that allows not only the sidereal tracking mode, but also the debris tracking.

Moreover, in the case of the first Italian observatory for space debris monitoring, it is required the semi-portability of the whole observatory.

All these requirements have been taken into account in the observatory design although considering that a main contractual drive of the project is the low economical budget.

2 THE OPTICAL TUBES

In general, the most important characteristic of an optical tube are:

- The diameter, therefore the resolution and the brightness;
- The focal length, therefore the FOV;
- The image quality;
- The transportability, if required by the project.

The image quality may be poor due to the optical configuration itself or to defects induced by poor manufacturing.

Taking into account what we said in section 1, we can say that, for the debris observation, the optics must have:

- a very short focal length to achieve a large FOV (allowing to survey a large region of the sky);
- a primary mirror diameter as large as possible (let say at least 300 mm) to see objects as small as possible;
- a configuration not heavily affected by aberrations.

The first two issues yield to a short focal length to aperture ratio. This is the main drive for the choice of all the optical configurations.

To take account of the semi-transportability, the weight of the optical tube cannot be too high: let say that a couple of people must be able to transport the optical tube.

Fig. 1: The Baker-Schmidt optical tube.

2.1 Baker-Schmidt tube

The project to have a focal ratio as small as possible yielded to the choice of the optical tube of the observatory, a Baker-Schmidt with a diameter of 300 mm and a focal ratio f/2.8 (Fig. 1).

The classical configuration of this telescope consists of a spherical primary mirror, a hyperbolic secondary mirror and a corrector plate to reduce the spherical aberration.

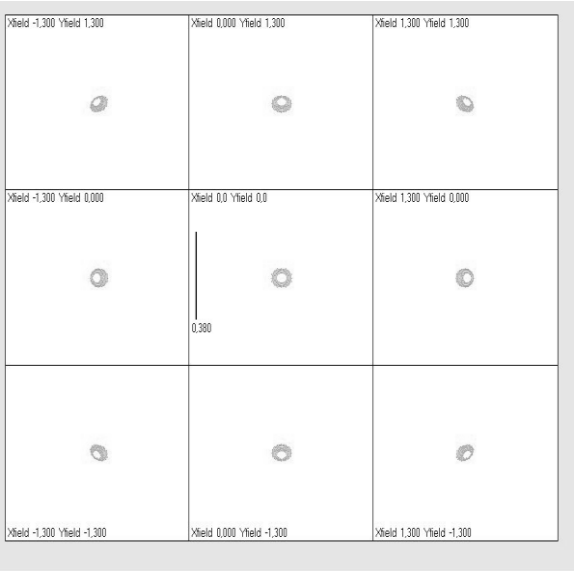

Fig. 2: Two-dimensional total field spot diagram for the 30 cm Baker-Schmidt optical tube, coupled with the 4K × 4K CCD.

Fig. 2 shows the two-dimensional total field spot diagram for the Baker-Schmidt tube: as it is apparent this optical tube is not affected by coma aberrations, while a small amount of spherical aberrations remain.

3 THE MOUNTS

Earth satellites tracking requires a fast tracking system.

We have chosen equatorial mounts, which easily compensate for Earth rotation, avoiding the rotation of the star field typical of alt-azimuthal mounts.

As the optical tubes are relatively light, a commercial mounts (described in the following sub-sections) could be chosen, avoiding the high cost of a specific design mount.

The mount is motorized with “Bisque TCS” Telescope Control System, a control hardware/software package, to be completed with a workstation (WS), which allows to accomplish the telescope pointing and the sky visualization, the automatic tracking planning, the CCD image acquisition and the remote control through the internet with client and server applications. On the other hand, the hardware alone can be used with specifically developed soft-ware for the telescope control.

3.1 Paramount GT1100

This is a very popular and appreciated equatorial mount used not only by amateur astronomers, but also by professionals when light OTAs have to be supported.

It is built of stainless steel and anodized aluminium; it weighs 45 Kg, without OTA and counterweights bar, and can support a load of 45 Kg. It can be interfaced with a workstation (WS) for fully autonomous operations. The fastest tracking speed is 5 deg/s for the right ascension engine, and 7 deg/s for the declination engine.

4 THE CCD CAMERAS

The observatory will be equipped with a CCD sensor. The choice of the sensor has been done with the following criteria:

1. The sensor should have been as large as possible, in order to have a FOV as large as possible. As the low-cost drive would have preclude any mosaic CCD assembly, the only feasible choice was procuring the largest CCD available off-the-shelf;

Typically the largest sensors have lower performances especially in terms of sensitivity (quantum efficiency) and pixel size. If a great pixel size is an advantage when looking for a great FOV or when observing faint objects (so that the same pixel can collect a greater number of photons), it is not fair when the greatest position determination accuracy is desired. Thus, for the CCD sensor is useful having quantum efficiency as high as possible and a pixel size as small as possible.

4.1 The ProLine CCD

The CCD sensor chosen among commercial cameras is the Kodak KAF 16803, featuring 4096 × 4096 pixels. In the following all the characteristics of the sensor are reported.

It is possible to see that the quantum efficiency (that is, the ratio between the revealed and incident photons at a certain wavelength) at 550 nm is the 60%, which is a relatively poor value. The pixel is a me-dium size one (9 μ m); however the total sensor dimension (38.6 × 37.76 mm) is the greatest we found off-the-shelf.

Parameters of the CCD sensor.

Number of Active Pixels 4096 (H) × 4096 (V) = 16.8Mp

Pixel Size 9 µm (H) × 9 µm (V)

Chip Size 38.6 mm (H) × 37.76 mm (V)

Saturation Signal 85 k e-

Quantum Efficiency (at 550 nm) 60%

Responsivity (at 550 nm) 1303 ke/µJ/cm², 28.7 V/µJ/cm²

Read Noise (f = 4 MHz) 9 e

Dark Signal 3 e/pix/sec

Dark Current Doubling Temperature 6.6 °C

Maximum Data Rate 10 MHz

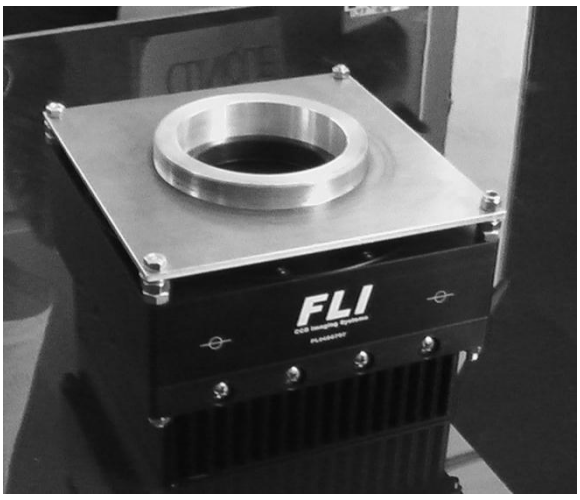

Fig. 3: FLI Proline 16803.

5 THE DOME

Generally, the dome of an observatory has an important role not only in the telescope protection, but even in isolating the instrument from the wind during the observations.

In the case of ASI observatory, a traditional semi-spherical dome was not suitable both for economical reasons and for the semi-portability requirement, which implies that the dome can be easily assembled and dismounted.

The structure is essentially made of a rectangular base with four quadrangular arcs rotating around a central axis in order to close the dome with a fabric cover, see Fig. 4 and Fig. 5.

Fig. 4: The dome open.

Fig. 5: The dome completely closed.

The transportability requirement was the main drive of the design. As a conse-quence, the main characteristic of the de-sign is the modularity: the structure consists of small, light parts, easy to transport and fast to assemble. Moreover, the modular

design allows the user to easily enlarge or reduce the dimensions of the dome − in case of future specific need − just by adding or removing some elements.

The structure is completely automated and it can be remotely controlled. An electric engine permits to open and close the structure in one minute.

While the framework is totally realized of Aluminium, the fabric material of the cover is Poly/450/PVC, a light and resistant material, which permits an easy deployment and an effective protection in most weather conditions.

6 THE ASSEMBLED OBSERVATORY

Fig. 6: The telescopes of the observatory.

Fig. 4 shows the telescopes inside the dome. The same telescope is better visible in Fig. 6: it has been assembled with the Paramount mount, the Baker-Schmidt optical tube and the FLI Proline 16803 CCD.

In Fig. 7 is reported the connection sketch for the observatory. A single portable WS (a laptop) is connected through serial and Universal Serial Bus (USB) connections to the CCD, the mount and the dome controller and the whole system can be remotely controlled via internet.

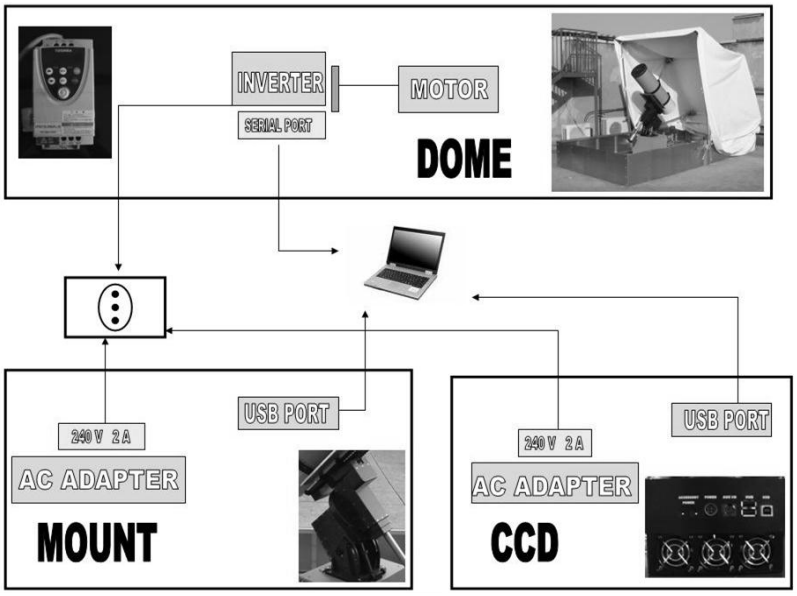

Fig. 7: Connection scheme for controlling the telescope of the SPADE observatory.

7 AUTOMATIC IMAGE PROCESSING

During the optical campaigns, a large number of images is expected to be archived. This is the reason why the software has been developed to process the images in order to automatically detect the objects and correlate them with the catalogue.

The algorithm is based mainly on single frame handling to make the noise level as flat as possible, with a successive two-image comparison, which allows removing stars and biases. The software also performs the object identification by comparing the actual position of the detected objects with the propagated positions of the catalogued ones.

The object identification is achieved by comparing the targets' measured positions with the propagated positions of catalogued objects.

8 POTENTIAL OF THE ORBIT DETERMINATION

Orbit determination for AI23.4 was performed by using null eccentricity hypothesis.

With the hypothesis of circular orbit, two optical measurements suffice to determine the remaining four orbital parameters: semi-major axis, inclination, right ascension of ascending node and the argument of latitude.

3. Description of observatory

All data was obtained with the SPADE Observatory located at Collepardo (IT) (longitude = 13 degrees Est, latitude = 45 54 degrees South, altitude = 500 meters).. The total field of view is about 2.0 x 2.0 square degrees. This telescope is not equipped with filter system. Since the purpose of this campaign is to go as faint as possible, and not to do colors, observing without a filter will not get problems.

The observatory observed fields suggested by coordinators. First night a section of sky close to the anti-solar point (but out of eclipse) for maximum reflected brightness was obsrved. The next night the telescope is offset by 1.2 degrees in declination (dec), and the observations are repeated at the same right ascension (ra). For the 2008 observing runs, since the Sun is moving North in declination, the anti-solar point is moving south, and so the nightly declination offsets are towards the south to keep as close to the anti-solar point as possible.

The observations were taken with sidereal tracking on to make easy the automatic object identification, this choice was due to the automation software and was preferred even if the faintest objects can be detected if the telescope tracks at the same rate as the object so that the object is detected as a point source, with most of its flux in the smallest number of pixels, and not as a streak and with stars will appear as streaks in these observations.

The observation mode we chose can be briefed as such several steps:

1. Point the telescope to the specified ra and dec

2.Turn the drive on.

3. Take exposures.

4. After 30 minutes correct for parallax

4. Observation results

It was observed for about 15 nights, But only data from 6 clear nights have been considered adapt to be inserted in the database, since other nights are corrupted by bad visibility.

During the analysed nights about 3000 frames were collected. About 150 objects were seen with about 1000 detections. The faintest magnitude of these detections can up to about 16. All magnitudes have not been reduced from apparent magnitudes to so-called absolute magnitudes by correcting for the illumination phase angle.

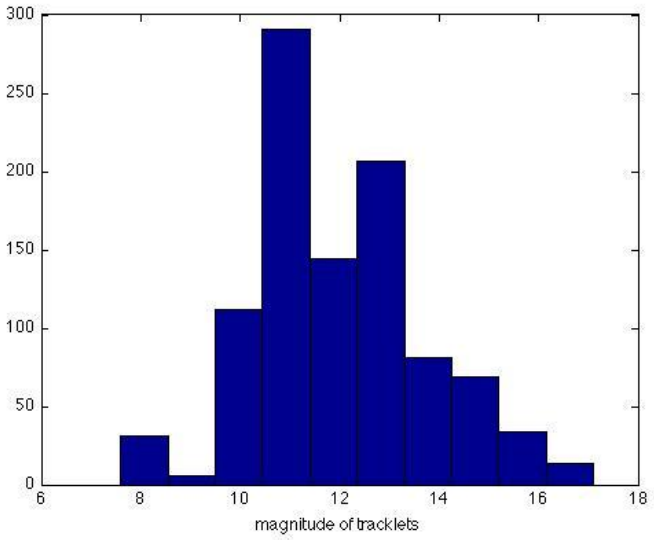

Fig.8 - Calibrated tracklets magnitude

Fig.8 shows the calibrated magnitude distribution of all tracklets detected. The magnitude didn't reduced from apparent magnitudes to so-called absolute magnitudes by correcting for the illumination phase angle. The accuracy is a few 0.1 magnitudes except someone which could rise to about 0.5.

Fig. 9 shows the calibrated magnitude for detected objects, the largest tracklet magnitude value was selected to identify the objects magnitude.

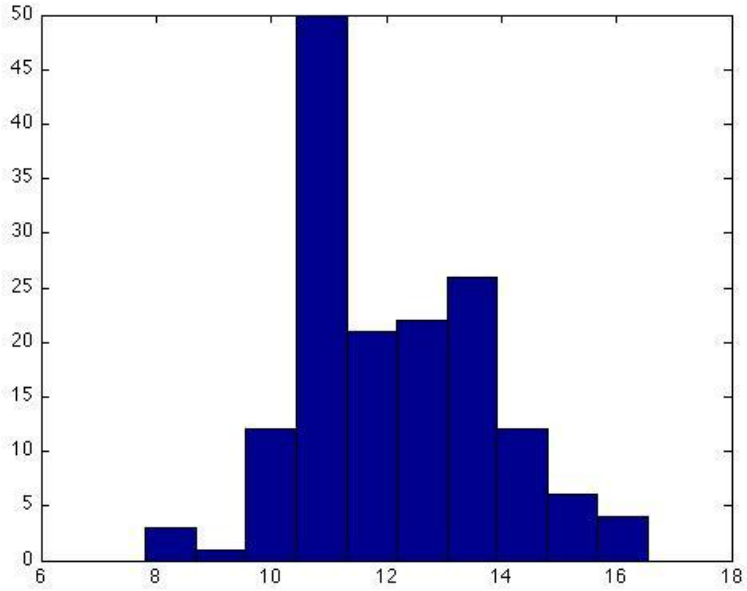

Fig.9 calibrated magnitude distribution for all objects

The inclination and semimajor axes distributions are shown in Fig. 10 and Fig. 11. Parameters for unidentified objects were achieved by using TLE and null eccentricity hypothesis.

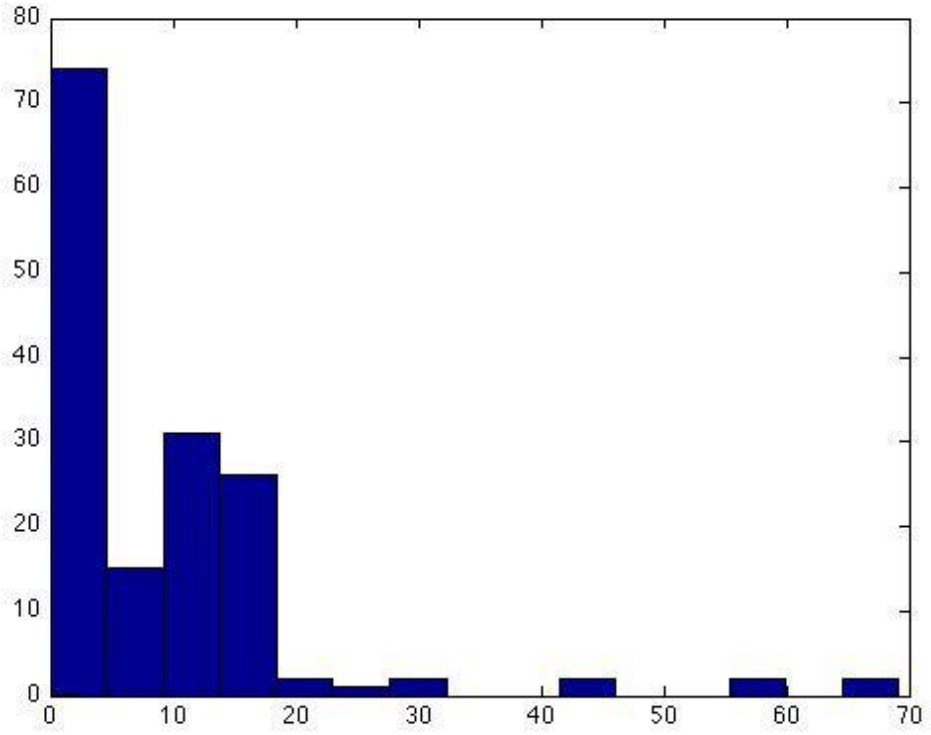

Fig. 10 Inclination distribution

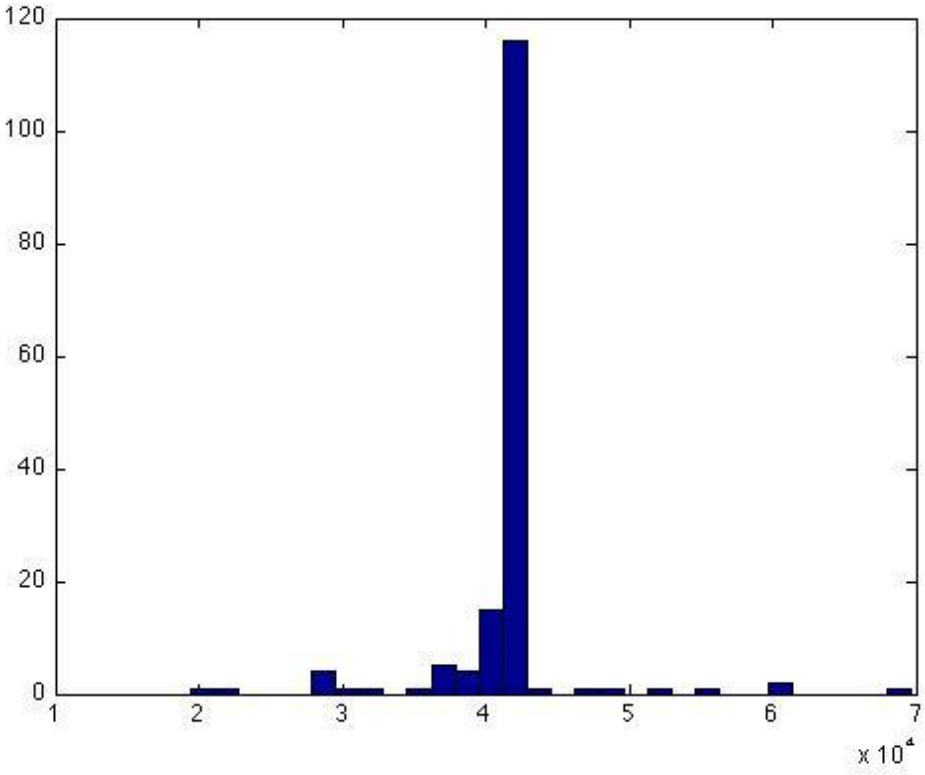

Fig.11 Semimajor axes distribution

The inclinations and right ascensions of the ascending nodes are strongly correlated, which can be shown in Fig.12 .

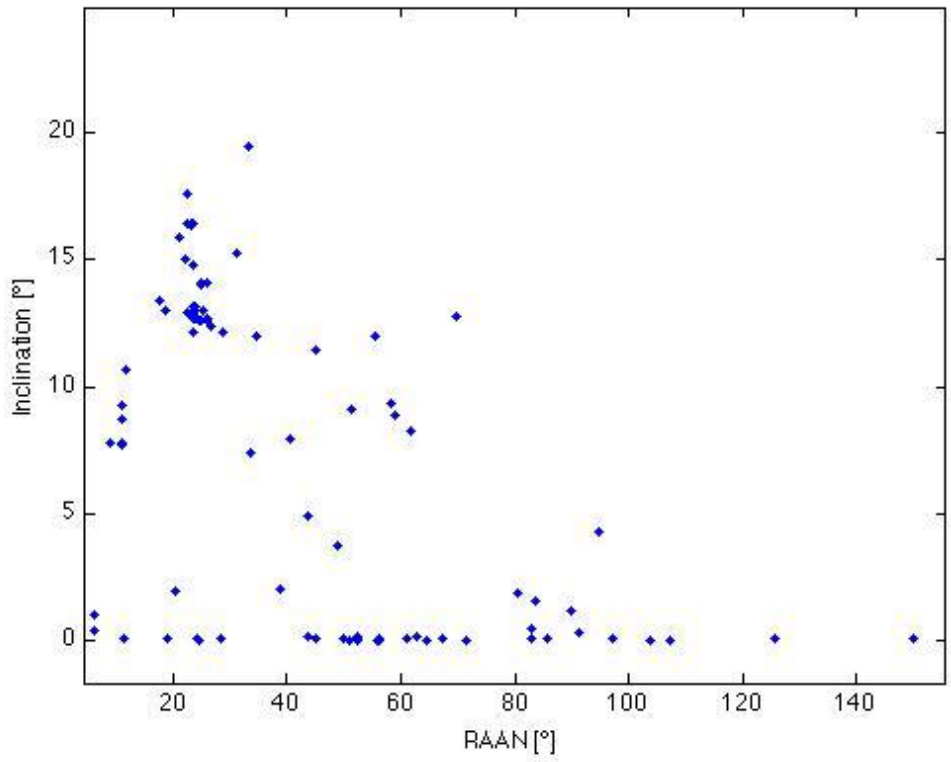

Fig.12 Inclination versus right ascension of ascending node

5. Discuss

The ASI telescope was designed for debris observation. All observing nights were ready to observe. Extremely bad weather conditions permitted to observe only during a few days, especially in May. Nevertheless a large number of trackletes were identified.

6. Acknowledgement

All of the work described here was supported by ASI and School of Aerospace engineering of University of Rome “LA Sapienza”. The observations were carried out by SPADE Telescope located at Collepardo.

CNES

CNES report on optical observations for IADC AI23.4

Etienne Ducrotté, Bruno Vidal, Pascal Richard

Centre National d'Etudes Spatiales, Toulouse, France

Bruno.Vidal@cnes.fr

Pascal.Richard@cnes.fr

Introduction

This document summarizes observations and results obtained by C.N.E.S., using the TAROT Calern telescope owned and operated by Observatoire de Haute Provence (OHP France), in the framework of IADC WG1 AI23.4 "International 2008 Optical Debris Campaign in Higher Earth Orbit". The goal of this action item is statistical studies of the debris population both at GEO and in the navigation satellite orbits with mean motions near 2 revs/day.

a) Description of the telescope and facilities used

TAROT telescopes are robotic observatories that observe with no human interaction. TAROT are two identical 25 cm telescopes F/D=3.4 that cover 1.86°x1.86° field of view on the Andor CCD cameras (Marconi 4240 back illuminated). Spatial sampling is 3.3 arcsec/pix. Six filters are available : BVRI, a clear filter and a 2.7 density coupled to V (for Moon and planets). Detection limit is about V=17 in 1 min. exposure. Locations of telescopes are:

- TAROT Calern observatory (France)
- TAROT La Silla ESO observatory : (Chile)

The principal investigator of these instruments is Michel Boër (Observatoire de Haute Provence, 04870 Saint Michel l'Observatoire, France). Two co-investigators are Jean-Luc Atteia and Alain Klotz, astronomers at the Observatoire Midi Pyrénées, Toulouse, France.

Observation requests are sent by observers through an internet interface or by the Gamma-ray Coordinates Network (GCN) through a socket. Planning is computed each time a new request is received. Telescope slewing is very fast, up to 60°/second, and read-out time of CCD cameras is only 5 seconds. When a GCN alert is received, the delay until the opening of the shutter is less than 8 seconds.

Raw images are automatically processed by TCL scripts runned by AudeLA software to provide reduced data ready use for researcher collaborators via web pages

TAROT telescopes are not only used for gamma ray bursts observations. They are also used by collaborators concerning many other scientific projects (http://tarot.obs-hp.fr/tarot/infos/), as well as educational programs.

Telescope Name		Tarot Calern
Main mission		Gamma Ray Burst Detection
Telescope Type		Automated telescope
Telescope data	Position	Observatoire de la Côte d'Azur (OCA) WGS84 coordinates : 43.7° N ; 6.9° E ; 1320 m
	Sensitivity	For a 10 seconds exposure, without filter, without moonlight : - for photometry : magnitude 14.9 (10 times the standard deviation of the background sky). - for astrometry : magnitude 16.2 (3 ?) For a 60 seconds exposure, without filter, without moonlight : - for photometry : magnitude 16.9 (10 ?) - for astrometry : magnitude 18.2 (3 ?)
	Optical scheme	Newton shaped, with hyperbolic M1 mirror
	Apperture diameter	250 mm
	Focal lenght	850 mm
	Camera type	CCD, Andor DW436S (Marconi 4240 back illuminated)
	Active pixels	2048 x 2048 pixels
	Image Area	27,6 x 27,6 mm
	Field of View	1.86 x 1.86 deg
	Pixel size	13.5 µm => 0.91 mdeg
	CCD temperature	225 K
	Wavelenght range	350 - 1000 nm
Mount Characterictics		Equatorial mount
		Pointing precision : 15 arcsec
		Pointing velocity : up to 40 deg/s

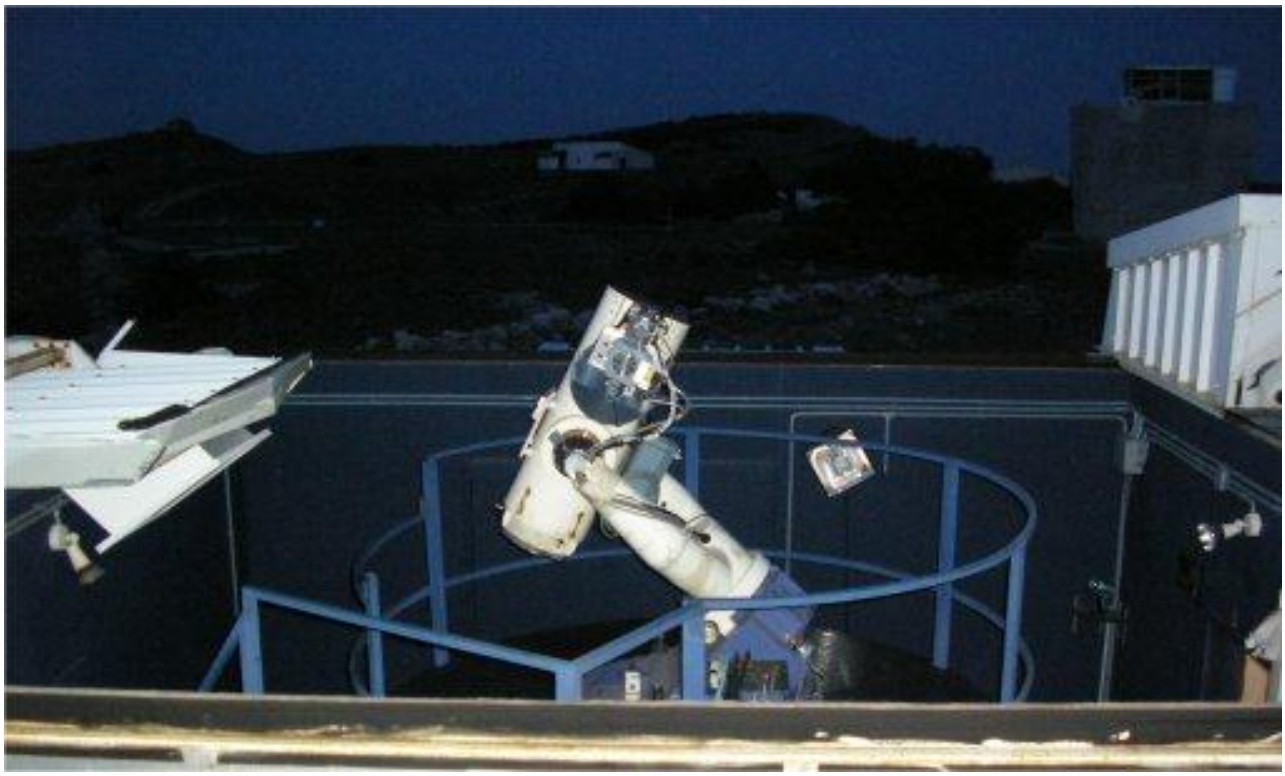

b) The observing method used

Filter : No filter were used, in order to maximize sensitivity

Observing routine (the time taken by a full cycle is about 90 seconds):

a. Compute the topocentric equatorial coordinates for the location given by the GEO regime semi major-axis and the target geocentric equatorial coordinates.

b. Repeat three times

   i. Point to computed topocentric equatorial coordinates.

   ii. Stop the drives

   iii. Take one exposure of 10 seconds

   iv. Readout the CCD

c) Data reduction method

Earth Satellites detection

Algorithm based on mathematical morphologies described in Myrtille Laas PhD Thesis: “Détection des satellites artificiels dans les images astronomiques: application aux images” (Université de Provence).

A dot or a streak on the image is considered as a detections if its flux is 7 times the standard deviation of the background sky.

False detection elimination

Rectilinear tracklets were constituted by software then visually validated and corrected. Dot detections that cannot be associated in tracklets of 3 measures were eliminated.

Detections of streaks were all kept.

Orbit computation

The orbit computation assumed circular orbit.

Apparent magnitude of objects

The apparent magnitude of objects was chosen as the median value of the apparent magnitudes of their observations. No correction was applied for atmospheric extinction or solar phase angle.

NORAD TLE correlation

the object identification is achieved by comparing the measured positions with the propagated positions of catalogued objects.

d) Calibration techniques

Astrometry

Differential astrometry based on Tycho 2 catalog. Accuracy is about 4 arcseconds.

Photometry

Six photographs (10, 10, 30, 30, 60 and 60 seconds) of a Landolt field near the target field were taken every 2 hours. Those photographs were not used for calibration. An empirical offset was applied on the photometric measures.

e) Summary of CNES results

The March to June observation rounds encountered respectively 3, 5, 6 and 2 good nights. We got a mean of 10 measures per detected object.

The tables and schemes below present:

- the nightly amount of object detections and USSTRATCOM TLE correlations,
- The distribution of observed instrumental magnitudes,
- Some characteristics of the orbital elements of detected objects.
- A synthesis of GEO and non GEO detections and correlations with USSTRATCOM TLE.

Nightly amount of detections and correlations

	Images	Measures	Objects	Correlated
March Summary	**1979**	**872**	**92**	**79**
April Summary	**4421**	**2197**	**230**	**162**
May Summary	**4081**	**3112**	**301**	**236**
June Summary	**1173**	**195**	**30**	**19**
Global summary	**11654 Images**	**6376 Measures**	**653 Objects**	**496 Correlated**

Distribution of apparent magnitudes for correlated and uncorrelated objects

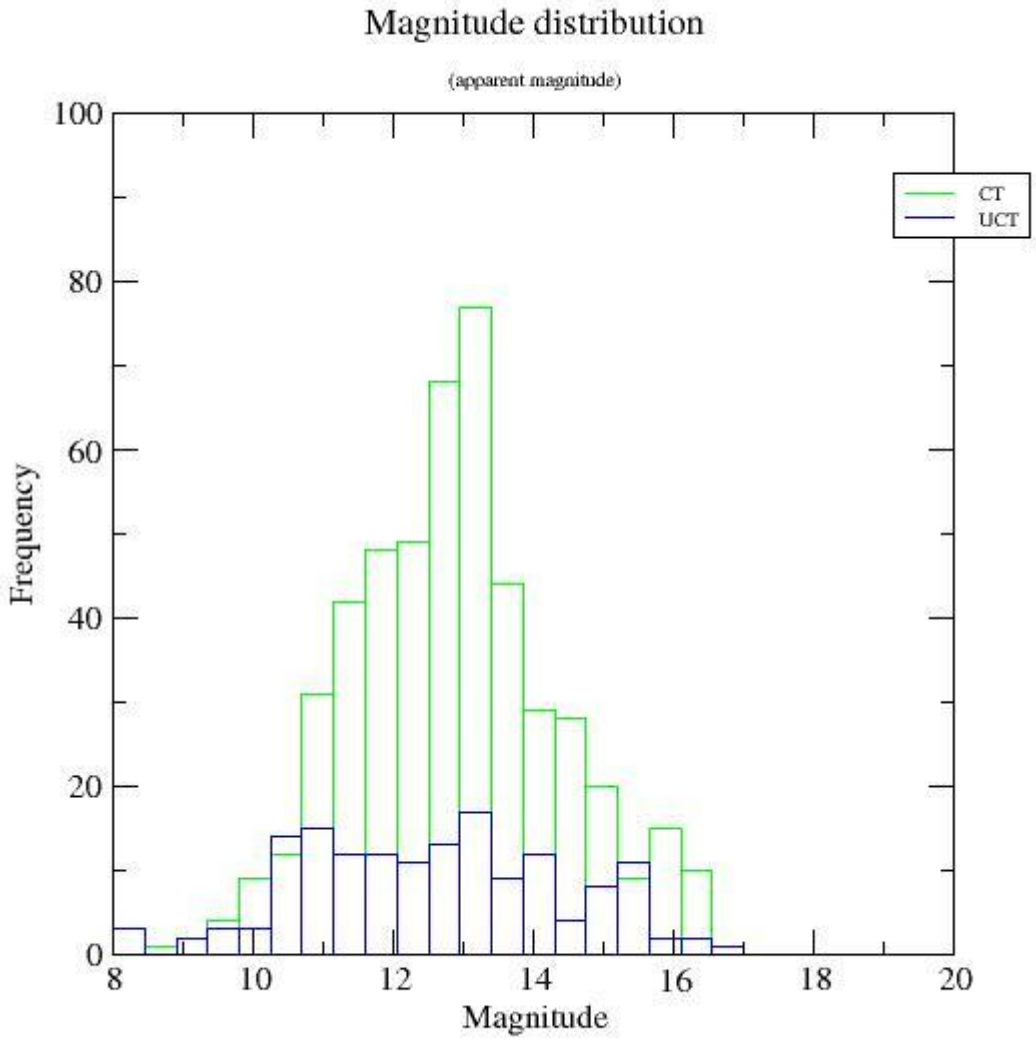

Distribution of inclinations of orbits for correlated and uncorrelated objects

Two regimes can be distinguished: GEO between 0 and 15°; MEO between 60 and 70°.

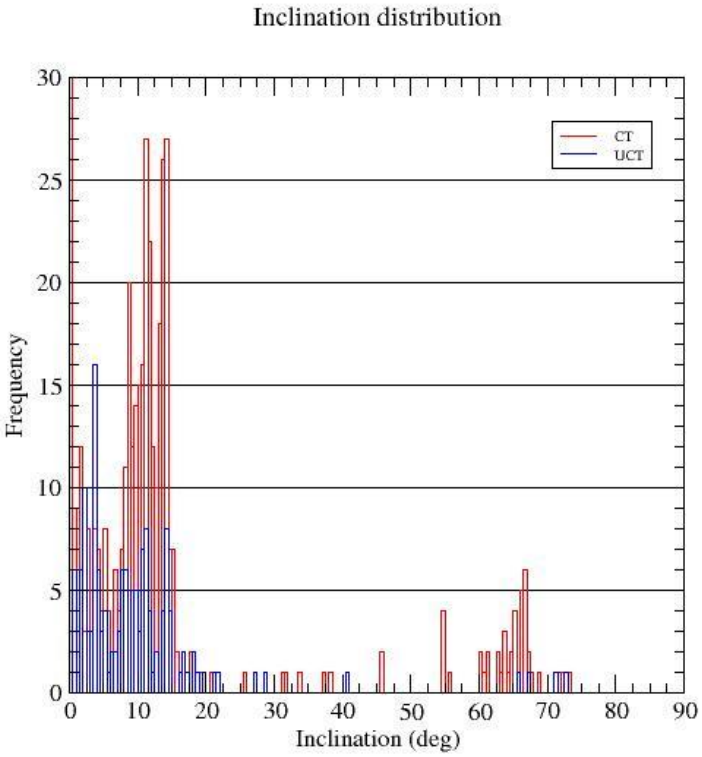

Inclination of orbits, function of the right ascension of their ascending node

The GEO regime and the MEO can be distinguished on this figure.

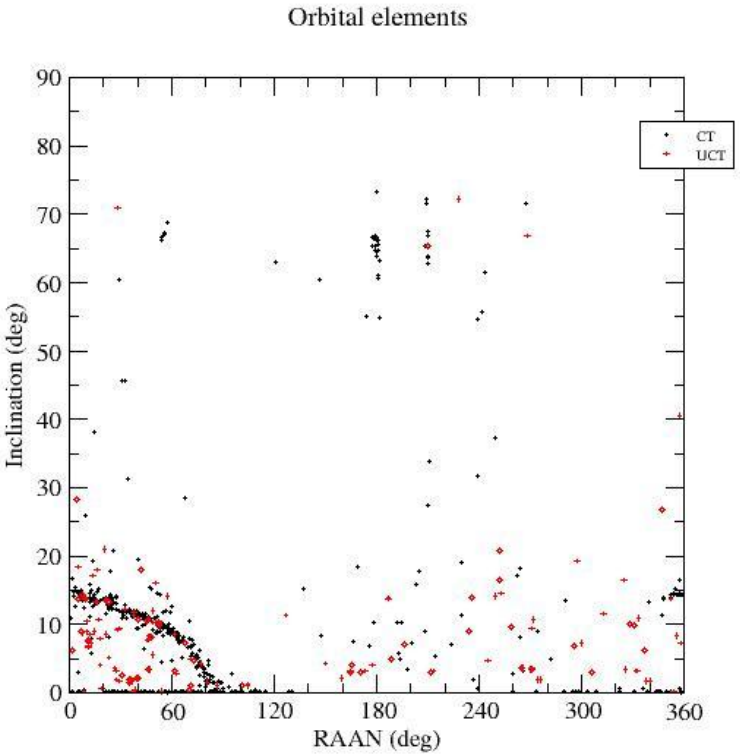

Semi major axis distribution

The two regimes MEO and GEO can be distinguished.

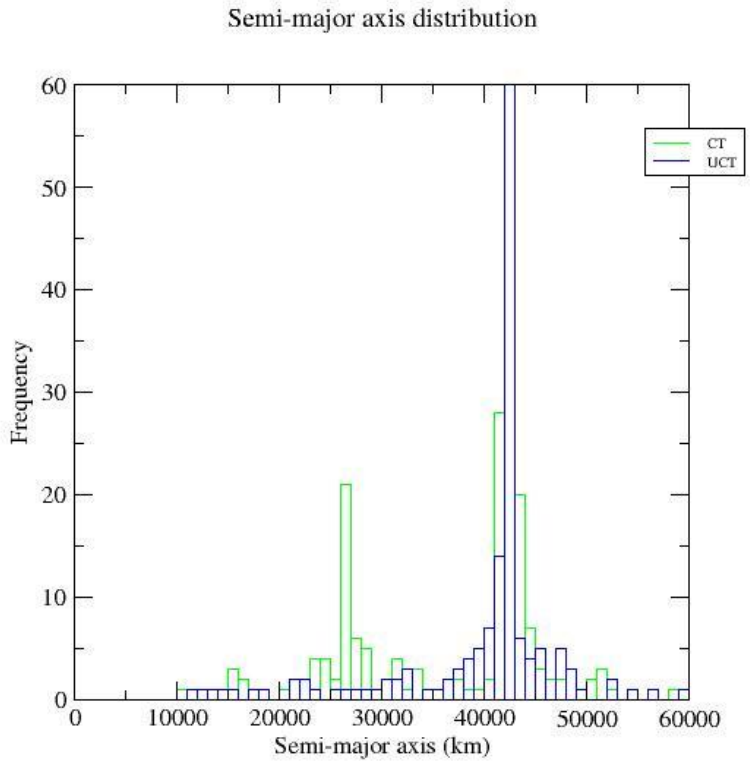

Synthesis of detections and correlations after GEO/MEO classification

GEO Satellites	**Measurements**	**Objects**	**UCT/CT (%)**
Correlated	4509	391	100
Uncorrelated	348	91	23

Non GEO satellites	**Measurements**	**Objects**	**UCT/CT (%)**
Correlated	1251	105	100
Uncorrelated	268	66	67

CNSA

Brief Report of PMO

Ping Yiding

Purple Mountain Observatory, Mail Code 210008, Nanjing, China

Email: ydping@pmo.ac.cn

Sun Rongyu

Purple Mountain Observatory, Mail Code 210008, Nanjing, China

Email: rysun@pmo.ac.cn

Wang Xin

Purple Mountain Observatory, Mail Code 210008, Nanjing, China

Email: wangxin@pmo.ac.cn

Zhao Haibin

Purple Mountain Observatory, Mail Code 210008, Nanjing, China

Email: meteorzh@pmo.ac.cn

Introduction

This document summarizes observations and results obtained by Purple Mountain Observatory in March 2008 of space debris at geosynchronous orbit (GEO) in support of WG1 Action Item 23.4, International 2008 Optical Debris Campaign in Higher Earth Orbit, organized by the Inter-Agency Space Debris Coordination Committee (IADC). The goal of this action item is statistical studies of the debris population both at GEO and in the navigation satellite orbits with mean motions near 2 revs/day. All of the work reported here was supported by Center for Space Object & Debris Research, CAS.

Description of observational techniques

All data was obtained with the PMO's CNEOS Telescope located at the Xuyi Observatory (longitude = 118。5 degrees West, latitude = 32.7 degrees South, altitude = 219 meters). Fig.1 shows the dome of this telescope. The CNEOS Telescope is a classical astronomical Schmidt telescope with 1.04 meter aperture. A 4k x 4k pixel CCD is equipped on the focal plane. The total field of view is about 2.0 x 2.0 square degrees and the pixel size is 1.7 arcseconds. This telescope is not equipped with filter system. Since the purpose of this campaign is to go as faint as possible, and not to do colors, observing without a filter will not get problems.

Fig.1 Dome of the PMO's CNEOS Telescope at the Xuyi Observatory.

The observing techniques to be used are consistent with previous IADC optical campaigns. This will permit comparison of the data obtained in this campaign with data from previous campaigns.

Previous IADC GEO campaigns observed a section of sky close to the anti-solar point (but out of eclipse) for maximum reflected brightness. The next night the telescope is offset by 1.2 degrees in declination (dec), and the observations are repeated at the same right ascension (ra). For the 2008 observing runs, since the Sun is moving North in declination, the anti-solar point is moving south, and so the nightly declination offsets are towards the south to keep as close to the anti-solar point as possible.

Table 1. Observing fields of March 2008. Change fields at 11h14m local sidereal time.

UT Date	RA (Field 1)	RA (Field 2)	Declination
4 Mar	10h14m	12h14m	8.40 deg
5 Mar	10h14m	12h14m	7.20 deg

6 Mar	10h14m	12h14m	6.00 deg
7 Mar	10h14m	12h14m	4.80 deg
8 Mar	10h14m	12h14m	3.60 deg
9 Mar	10h14m	12h14m	2.40 deg
10 Mar	10h14m	12h14m	1.20 deg

The faintest objects can be detected if the telescope tracks at the same rate as the object so that the object is detected as a point source, with most of its flux in the smallest number of pixels, and not as a streak. Stars will appear as streaks in these observations.

However, not all GEO objects travel at the same rate and thus some objects will appear as short streaks. In order to keep streak losses low, the exposure times are kept short (typically a few seconds).

The observation mode we chose can be briefed as such several steps:

1. Point the telescope to the specified ra and dec

2.Turn the drive off.

3. Take a single exposure.

4. Reset the telescope to the first ra and dec.

5. Repeat the process for the time period of the observations.

Each clear night, we takes a 5 second exposure every about 40 seconds at a constant right ascension and declination. Typically over 700 images are obtained each night. During the 8 minutes that it takes a GEO object to drift across the field of view, up to 12 independent detections of each source are made.

Fig.2 shows a representative image from a typical observing sequence. Three active satellites are visible.

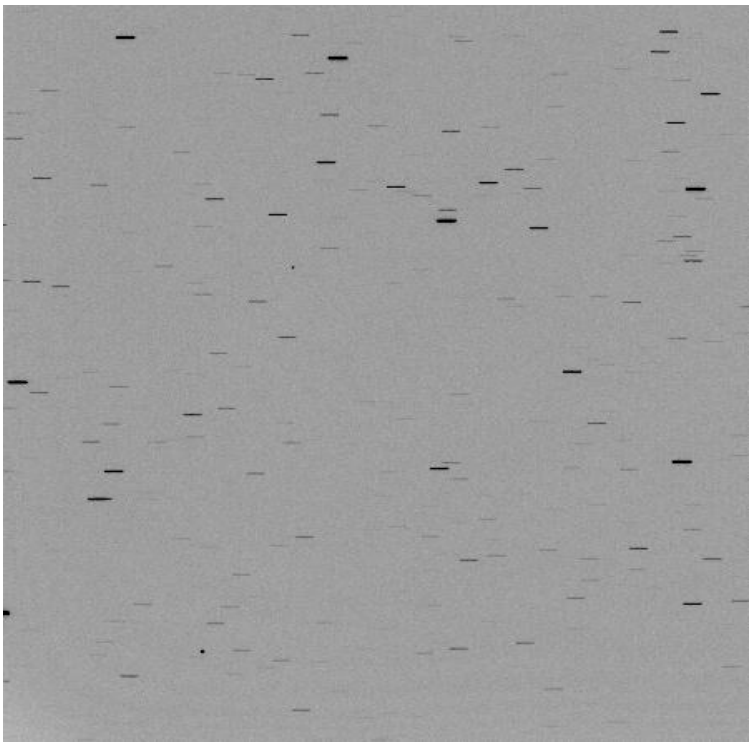

Fig.2 PMO CNEOS Telescope's example image, which is a 5 second exposure, obtained on the geostationary belt. There are 2 stationkeeping satellites in the image. The short streaks are remnants of star subtraction.

Observational results

In 5 clear nights, we conducted the observations with the CNEOS Telescope. Table 2 gives the overview of these observations. Above 2500 observation detections were identified to be the space debris. The faintest magnitude of these detections can up to about 19. All magnitudes have not been reduced from apparent magnitudes to so-called absolute magnitudes by correcting for the illumination phase angle.

Table 2. PMO Observations

Date	Frames	Observe Time	Image Data	Observed detections
04/03/2008	100	3 hours	3.2GB	39
05/03/2008	550	6 hours	17.6GB	830
07/03/2008	550	5hours	17.6GB	594
09/03/2008	600	5hours	19.2GB	669
10/03/2008	550	6hours	17.6GB	534

Table 3 shows the detections overall, within which there may be some detections refer to the same object. All of the objects do not correlate with the catalogue.

Table 3. PMO GEO Sruvey

Date	Frames	Observe Time	Image Data	Detections
03/2008	2500	5nights/28h	80GB	1217

Fig.3 shows the calibrated magnitude distribution of all objects detected. The magnitude didn't reduced from apparent magnitudes to so-called absolute magnitudes by correcting for the illumination phase angle. The accuracy is a few 0.1 magnitudes except someone which could rise to about 0.5.

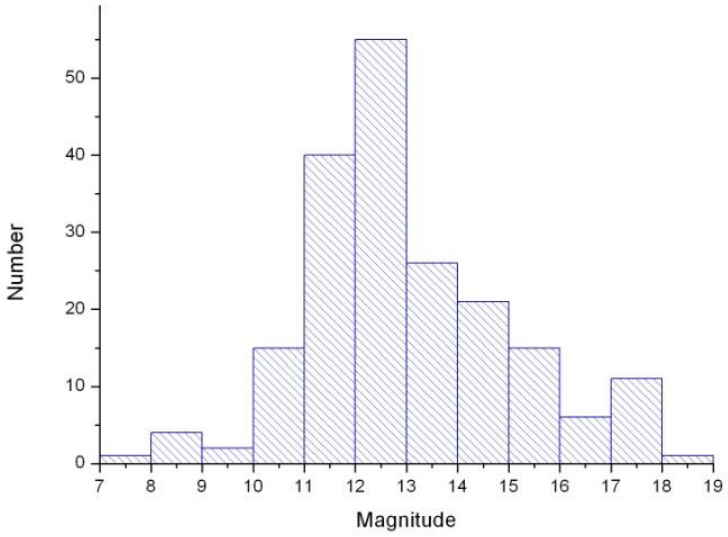

Fig.3 calibrated magnitude distribution for all objects

The inclination and semimajor axes distributions are shown in Fig. 4 and Fig. 5. Optical surveys are inherently designed such that the objects are detected on a short series of a few frames. The total time interval of these series is of the order of a few minutes. These short arcs of angle-only data force us to determine circular orbits.

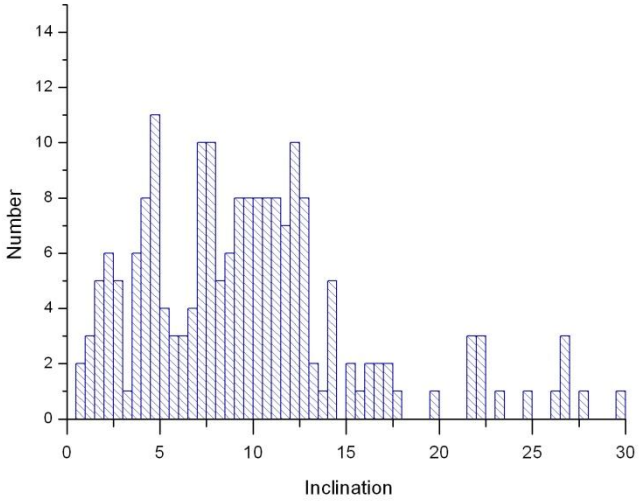

Fig.4 Inclination distribution

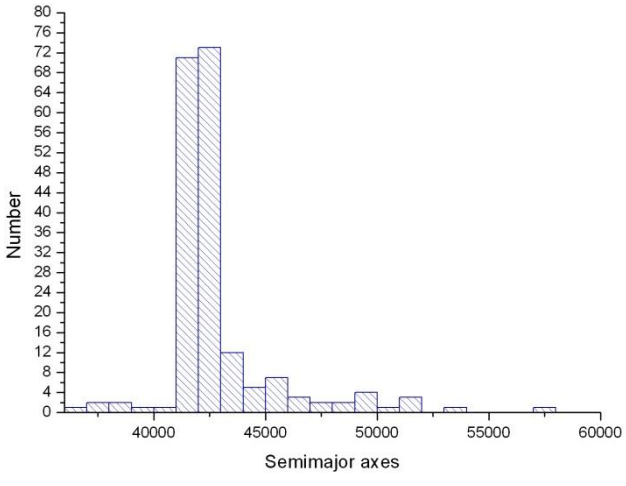

Fig.5 Semimajor axes distribution

The inclinations and right ascensions of the ascending nodes are strongly correlated, which can be shown in Fig.6 .

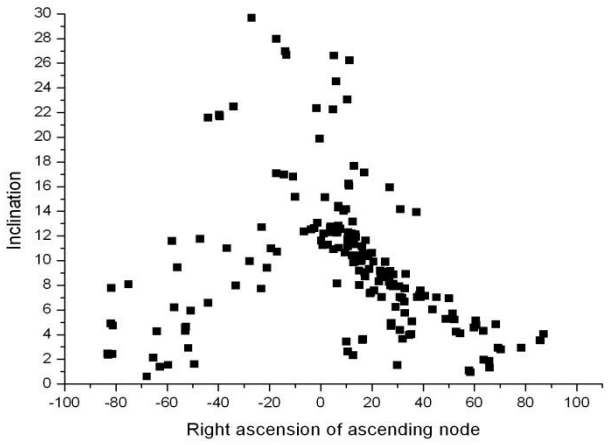

Fig.6 Inclination versus right ascension of ascending node

Discussion

The CNEOS telescope was not designed for debris observation, many sources do not have adequate independent detections for orbit determination. This problem make the following data analysis work become infeasible. A 90cm telescope designed for debris observation is being developed now. The routine GEO debris survey will be done by this telescope in China, and we will carry out the IADC campaign perfectly.

Acknowledgement

All of the work described here was supported by Center for Space Object & Debris Research, CAS. The observations were carried out by PMO's CNEOS Telescope located at the Xuyi Observatory, with the help of Dr. Zhao Haibin.

ESA

ESA REPORT TO THE IADC FOR

AI 23.4 INTERNATIONAL 2007 OPTICAL DEBRIS CAMPAIGN IN HIGHER EARTH ORBIT

T. Schildknecht[1], A. Vananti[1], H. Krag[2], H. Klinkrad[2]

(1) Astronomical Institute, University of Bern AIUB, Sidlerstrasse 5, CH-3012 Bern, Switzerland
(2) ESA Space Debris Office, ESOC, Robert-Bosch-Strasse 5, DE-64293 Darmstadt, Germany

Version 1.0

Bern, September 2010

1 INTRODUCTION

This report summarizes the ESA observations and results obtained in support of the IADC International 2007 Optical Debris Campaign In Higher Earth Orbit. All observations were acquired at the ESA 1-meter Space Debris Telescope (ESASDT) at the Teide Observatory at Tenerife, Canary Islands, Spain. The purpose of this campaign was to continue statistical monitoring of 8+ hour period orbital regimes during four one-week windows in duration.

2 DESCRIPTION OF OBSERVATION TECHNIQUES

2.1 The Observatory

The ESA Space Debris Telescope is installed at the Teide Observatory Izaña (2393 m) in Tenerife, Canary Islands (Figure 2-1).

Figure 2-1: Dome of the ESA Space Debris Observation Telescope at the Teide Observatory Izaña (2393 m) on Tenerife, Canary Islands. The Teide volcano (3,715 m) can be seen in the background .

ESA's Space Debris Telescope made by Carl Zeiss Jena is a classical astronomical telescope with a 1-meter primary mirror and an English mount (Figure 2-2). For debris observations the modified Ritchey-Chrétien focus is equipped with a CCD camera. The focal plane array consists of a mosaic of four 2k x 2k pixel CCDs. The total field of view is about 0.7 x 0.7 square

degrees and the pixel size corresponds to 0.6 arcseconds. The CCDs are cooled with liquid nitrogen to 160 K to reduce the dark signal produced by thermal motion.

At the typical exposure time of 2 seconds, the system allows the detection of 20–21 magnitude objects.

Figure 2-2: ESA Space Debris Telescope.

2.2 The Observation Campaigns

2.2.1 Observation campaign details

The coordinated IADC campaign asked for specific GEO survey fields to be observed during each night. ESA acquired data for the IADC 23.4 international debris campaign during a total of 21 of the 37 planned observation nights. A summary for the IADC observation nights at the ESA space debris telescope is given in Table 2-1.

ESA was combining the IADC search fields with fields of its ongoing survey campaigns in GEO and GTO, as well as with the necessary observations to maintain its catalogue of small-size debris. All ESA IADC surveys consisted therefore of a mixture of the IADC GEO fields, ESA GEO and GTO surveys fields, and follow-up observations of newly detected objects and of catalogued objects. The results presented in this report stem from both, surveys of IADC fields and from surveys of ESA GEO and GTO fields.

UT Date	RA (1)	RA (2)	Declination	Remarks
5 Feb	08h20m	10h20m	14.40 deg	no IADC obs.
6 Feb	08h20m	10h20m	13.20 deg	no obs. (wind too high)
7 Feb	08h20m	10h20m	12.00 deg	bad weather
8 Feb	08h20m	10h20m	10.80 deg	no obs. (wind too high)
9 Feb	08h20m	10h20m	9.60 deg	humidity too high
10 Feb	08h20m	10h20m	8.40 deg	humidity too high
11 Feb	08h20m	10h20m	7.20 deg	good
4 Mar	10h14m	12h14m	8.40 deg	no IADC obs.
5 Mar	10h14m	12h14m	7.20 deg	good
6 Mar	10h14m	12h14m	6.00 deg	good
7 Mar	10h14m	12h14m	4.80 deg	good
8 Mar	10h14m	12h14m	3.60 deg	software problem
9 Mar	10h14m	12h14m	2.40 deg	good
10 Mar	10h14m	12h14m	1.20 deg	no telescope time
2 April	12h02m	14h02m	3.60 deg	good
3 April	12h02m	14h02m	2.40 deg	no obs. (wind too high)
4 April	12h02m	14h02m	1.20 deg	good
5 April	12h02m	14h02m	-1.20 deg	good
6 April	12h02m	14h02m	-2.40 deg	no obs. (wind/hum. too high)
7 April	12h02m	14h02m	-3.60 deg	good
8 April	12h02m	14h02m	-4.80 deg	no obs. humidity too high)
1 May	13h52m	15h52m	0.0 deg	good (some clouds)
2 May	13h52m	15h52m	-1.2 deg	no obs. (technical problems)
3 May	13h52m	15h52m	-2.4 deg	good (some clouds)
4 May	13h52m	15h52m	-3.6 deg	good
5 May	13h52m	15h52m	-4.8 deg	good
6 May	13h52m	15h52m	-6.0 deg	good
7 May	13h52m	15h52m	-7.2 deg	no obs. (clouds)
8 May	13h52m	15h52m	-7.2 deg	no obs. (clouds)
9 May	13h52m	15h52m	-7.2 deg	good
30 May	15h45m	17h45m	-8.4 deg	good (humidity high)
31 May	15h45m	17h45m	-9.6 deg	good
1 June	15h45m	17h45m	-10.8 deg	good
2 June	15h45m	17h45m	-12.0 deg	good (partial night only)
3 June	15h45m	17h45m	-13.2 deg	good (partial night only)
4 June	15h45m	17h45m	-14.4 deg	no IADC obs.
5 June	15h45m	17h45m	-15.6 deg	good (partial night only)

Table 2-1: Summary for the IADC observation nights at the ESA space debris telescope. The 'RA'/'DEC' refer to the survey field geocentric coordinates. 'RA(1)' was used before and 'RA(2)' after local midnight. During the last campaign from June 2 to 6 the telescope was only partially available due to software tests.

The observation time for the IADC surveys, the ESA GEO/GTO surveys, and the follow-up observations for each 1-week sub-campaign is provided in Table 2-2. The column 'IADC' refers to IADC surveys, 'GEO' refers to ESA GEO surveys, the columns 'GTO-75' and

'GTO-105' to two types of GTO surveys. Although optimized for objects in low inclination GTO, the latter surveys are also sensitive to objects in the GEO region but my have a slightly reduced limiting magnitude for these objects.

Sub-campaign	Obs. nights		Observation Time [h]					
	Total	IADC	Total	IADC	GEO	GTO75	GTO105	follow-up
svyfeb08	2	1	12.3	1.5	2.4	1.9	1.3	5.3
svymar08	8	4	33.9	4	5.4	12.0	0.0	12.5
svyapr08	7	4	29.4	6.5	1.3	0.0	8.2	13.4
svymay08	8	6	50.5	12.1	3.9	14.4	0.0	20.2
svyjun08	12	6	51.7	5.9	5.6	0.0	11.4	28.8
Total	37	21	177.8	30	18.6	28.3	20.9	80.2

Table 2-2: Summary of observation sub-campaigns which included IADC observations. 'IADC' refers to IADC surveys, 'GEO' refers to ESA GEO surveys, 'GTO-75' and 'GTO-105' to two types of GTO surveys and 'follow-up' to the follow-up observations.

2.2.2 Survey fields

The fields covered by the observation sub-campaigns which included IADC observations are given in Figure 2-3 to Figure 2-5. The figures show the survey fields of the February to June 2008 sub-campaigns (small squares) in the right ascension-declination space as seen from the geocenter. The gray-shaded background indicates the apparent density of the catalogued GEO objects (TLEs from April 2008). Figure 2-3 includes all fields, Figure 2-4 shows the ESA GEO and GTO fields, and Figure 2-5 includes only the IADC fields.

Figure 2-3 to Figure 2-5 do not indicate which (or how many) objects should be observable in a given field, but merely which orbital planes we may see in a particular field. A geostationary object in an orbital plane crossing a given survey field will cross this field once every day, but perhaps when the field is not visible from the OGS (this is in particular the case for GEO objects at longitudes not accessible from Tenerife).

Note that in the Planning Tool all survey fields are defined by the geocentric positions of their field centers. These positions are transformed to topocentric positions (i.e., the parallax is applied) only when the short term plan, i.e., the sequence of telescope and camera commands is generated. This ensures that survey series of the same survey field always sample the same region in GEO regardless of any parallax effect.

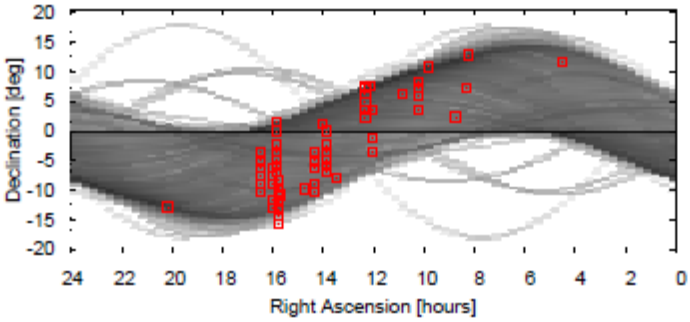

Figure 2-3: Survey fields of the February to June 2008 sub-campaigns (small squares) in the right ascension-declination space as seen from the geocenter. The gray-shaded background indicates the apparent density of the catalogued GEO objects (TLEs from April 2008).

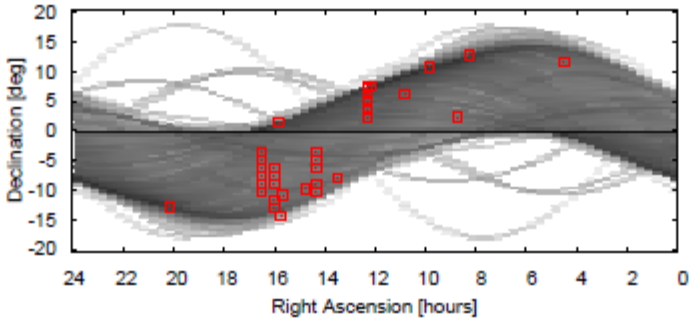

Figure 2-4: ESA GEO and GTO survey fields of the February to June 2008 sub-campaigns (small squares) in the right ascension-declination space as seen from the geocenter. The gray-shaded background indicates the apparent density of the catalogued GEO objects (TLEs from April 2008).

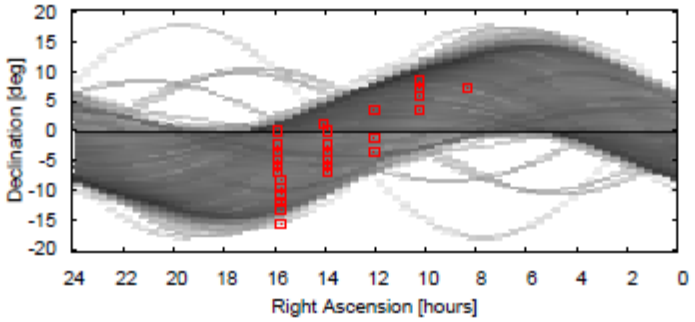

Figure 2-5: IADC survey fields of the February to June 2008 sub-campaigns (small squares) in the right ascension-declination space as seen from the geocenter. The gray-shaded background indicates the apparent density of the catalogued GEO objects (TLEs from April 2008).

2.3 Results from the Surveys

All four survey types (IADC, ESA GEO, GTO-75, GTO-105) are sensitive to both, GEO and GTO objects. The differences in sensitivity for the different object types are in most cases of less than one astronomical magnitude. We thus do not expect significantly different results for the IADC and the other survey fields in terms of object types, which were discovered.

In the following sections we present the results using the combined data from all survey types, as well as the results from the IADC survey fields only. Table 2-3 gives an overview on the objects detected in alls fields and in the IADC survey fields. The terms 'correlated' and 'uncorrelated' detections refer to detections for which a corresponding catalogue object could or could not be identified, respectively. The identification procedure, or 'correlation procedure', is based on comparing the observed orbital elements and the observed position in longitude and latitude of the object at the observation epoch with the corresponding data from the catalogue. We used the unclassified part of the USSTRATCOM catalogue as our reference (actually data from the ESA DISCOS database was used). By 'detection' we denote the detection of an object within a single 30- or 15-minute observation series. Some of these detections may actually refer to the same object, i.e., we may have incidentally re-observed some of the objects previously.

It is important to point out that all surveys in Table 2-3 suffer from observational biases depending on observation epochs and pointing directions at these epochs ('what we see depends on where and when and how we look'). The numbers given in Table 2-3 could therefore be misleading, e.g., when simply taking the ratio of uncorrelated to correlated detections as a measure to estimate the total number of debris objects!

	Nights	Total Observation Time [h]	Correlated detections	Uncorrelated detections
Feb – Jun 2008 IADC/GEO/GTO	37	97.6	163	288
Feb – Jun 2008 IADC	21	30	48	98

Table 2-3: Overview on the objects detected in alls fields and in the IADC survey fields.

2.3.1 Absolute magnitude distribution

Figure 2-6 shows the distribution of absolute magnitudes for the detections from all survey fields of the February to June 2008 sub-campaigns (IADC, ESA GEO, and GTO fields combined). The results for the data subsets including the IADC fields only is given in Figure 2-7. The solid lines indicate the system sensitivity (scale at right-hand side) as determined from independent calibration measurements. All magnitudes have been reduced from apparent magnitudes to so-called absolute magnitudes by correcting for the illumination phase angle. For the scattering properties we assumed a simple Lambertian sphere. No reduction to a common distance has been done because of the uncertainties of the determined orbits (see below). The value of this correction would be below 0.5 magnitudes in most cases. The magni-

tudes are astronomical 'V magnitudes' and have an accuracy of a few 0.1 magnitudes, except for the very faint objects where errors could amount to a maximum of 1 magnitude. The indicated object sizes were derived by assuming Lambertian spheres and a Bond albedo of 0.08. Both assumptions, however, are uncertain, as long as we do not know the nature of the observed objects.

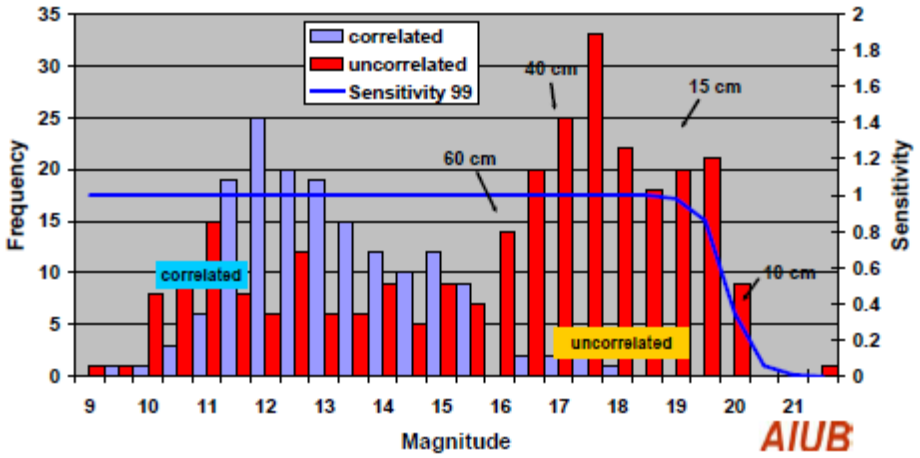

Figure 2-6: Absolute magnitude distribution for the detections from all survey fields of the February to June 2008 sub-campaigns (IADC, ESA GEO, and GTO fields combined). The solid line indicates the system sensitivity (scale at right-hand side) as determined from independent calibration measurements.

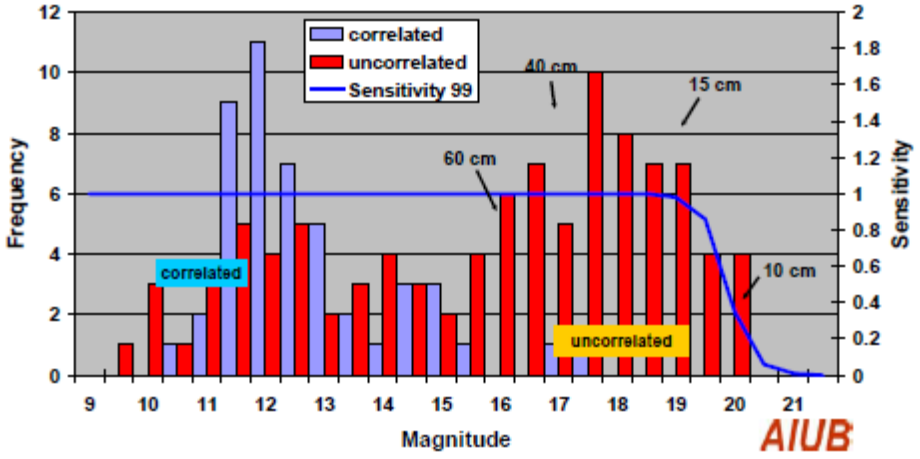

Figure 2-7: Absolute magnitude distribution for the detections from the IADC fields of the February to June 2008 sub-campaigns. The solid line indicates the system sensitivity (scale at right-hand side) as determined from independent calibration measurements.

The distribution is bimodal and very similar for both data sets. The distribution of the correlated objects has its peak at about magnitude 12 and spreads from about magnitude 10 to 16. It is also slightly asymmetric with the slope on the fainter end being shallower. This distribution nicely (and to some extent naturally) reflects the size distribution in the catalogue. The uncorrelated objects seem to be concentrated in a broad strong peak around magnitude 17 to 19 and in a second much less pronounced peak, which follows more or less the distribution of correlated objects.

The bright objects in the latter peak are most likely all 'known', large objects, which did not correlate with the catalogue for several reasons: Only inferred circular orbits have been determined and objects in eccentric orbits like GTO and high area-to-mass ratio (AMR) GEO objects can therefore not be correlated. Furthermore, some of these objects are classified and were therefore not included in the 'unclassified' version of the catalogue. Others might well be in the catalogue but did not correlate due to insufficient accuracy of the catalogue or due to a recent maneuver of the object not yet reflected by the catalogue at the time of observation. In some cases these objects are members of groups of satellites co-located in the same 0.1-degree longitude slot. They often correlate with several objects in the catalogue, again due to the limited accuracy of the catalogue, and thus end up as 'uncorrelated'. Also the catalogue most likely is incomplete at its fainter end.

The uncorrelated objects in the range from magnitude 15 to 21 are smaller than the minimum size of the objects in the catalogue. The apparent main peak of this population at about magnitude 18 is in fact not a peak, because the cutoff in the number of objects fainter than about magnitude 19 is entirely due to the sensitivity limit of the observation system (see the line indicating system sensitivity). The real distribution beyond magnitude 19 could therefore still increase!

2.3.2 Distribution of semimajor axes

Figure 2-8 shows the distribution of the so-called 'inferred' semimajor axes for the detections from all survey fields of the February to June 2008 sub-campaigns (IADC, ESA GEO, and GTO fields combined). The corresponding results for the IADC field only are given in Figure 2-9. By the term 'inferred' we denote that these semimajor axes are in fact the radii of the circular orbits determined from the detection observations (the extremely short arc of the detection observations does not allow for a full 6-parameter orbit determination). Again, the distribution for the two data subsets is very similar. Both, the correlated and the uncorrelated objects are concentrated around the nominal GEO semimajor axis. The semimajor axes of the uncorrelated objects, however, are much more dispersed showing a significant asymmetry with excess at large values. The last bin at 50'500 km in fact contains all detections with semimajor axes larger than 50'000 km.

I It is important to keep in mind that inferred semimajor axes are determined assuming circular orbits, which is certainly not the best guess for all objects. In general, fixing the eccentricity at a wrong value may result in a large bias of the inferred semimajor axis. Part of the spread for the uncorrelated objects as well as some of the large values may be due to this effect. Objects on highly eccentric orbits having their apogee near GEO may mimic objects in much higher circular orbits when observed at apogee. This is in particular the case for objects on a geostationary transfer orbit (GTO). Fitting circular orbits through observations of GTOs near apogee yields inferred semimajor axes of the order of 50000 kilometers, whereas the real

values would be about 26000 kilometers but with an eccentricity of e=0.73. But also observations from high AMR GEO objects can result in inferred semimajor axes clearly larger than the nominal GEO radius.

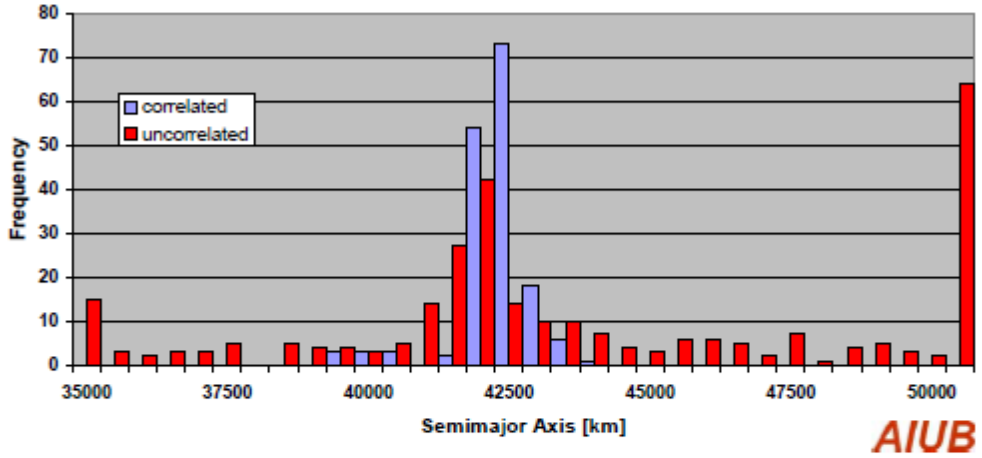

Figure 2-8: Distribution of inferred semimajor axes for the detections from all survey fields of the February to June 2008 sub-campaigns (IADC, ESA GEO, and GTO fields combined).

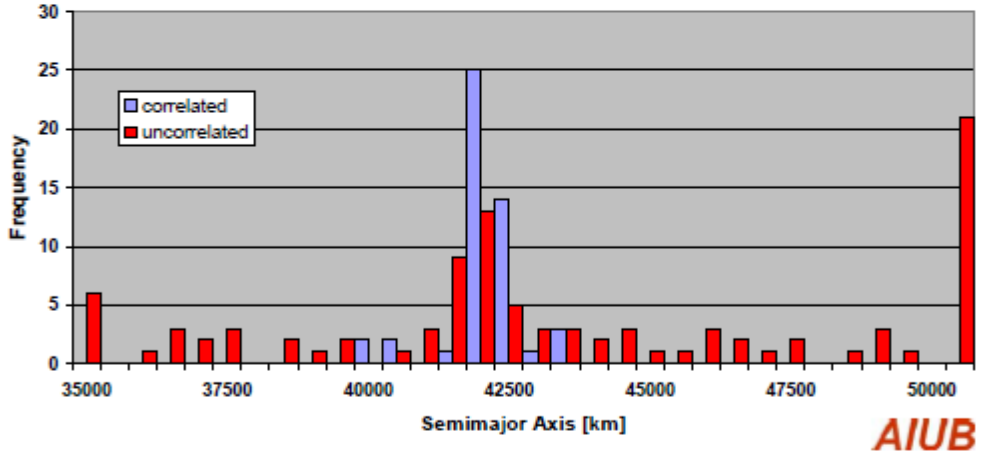

Figure 2-9: Distribution of inferred semimajor axes for the detections from the IADC fields of the February to June 2008 sub-campaigns.

2.3.3 nclination and right ascension of the ascending node

Due to the precession of the orbital planes of GEO objects around the Laplacian plane the inclinations i and right ascensions of the ascending nodes Ω are strongly correlated for the TLE population. Figure 2-10 and Figure 2-11 give both elements for all correlated and uncorrelated

detections from all survey fields and from the IADC survey fields only. The distinct curve followed by the correlated objects is caused by the 53-year precession period of the orbital planes. Assuming that the objects started with orbits of $i = 0°$ inclination the actual position in the diagram stands for the time since the end of active inclination control. The orbits gradually evolve from low inclinations and at right ascensions of the ascending nodes of about 90 to 100 degrees to higher inclinations and smaller right ascensions of the nodes until they reach the maximum inclination of $i = 15°$ after 26.5 years. The oldest catalogue objects have already passed this point.

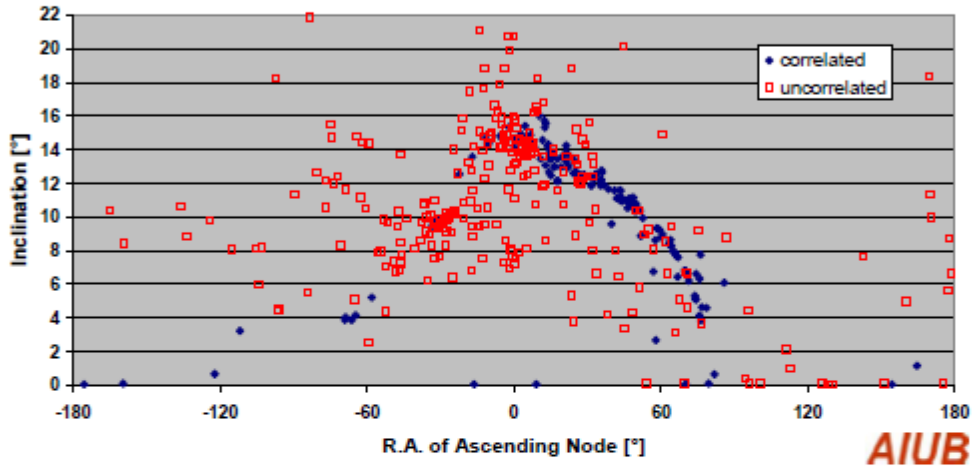

Figure 2-10: Inclination versus right ascension of ascending node for the detections from all survey fields of the February to June 2008 sub-campaigns (IADC, ESA GEO, and GTO fields combined).

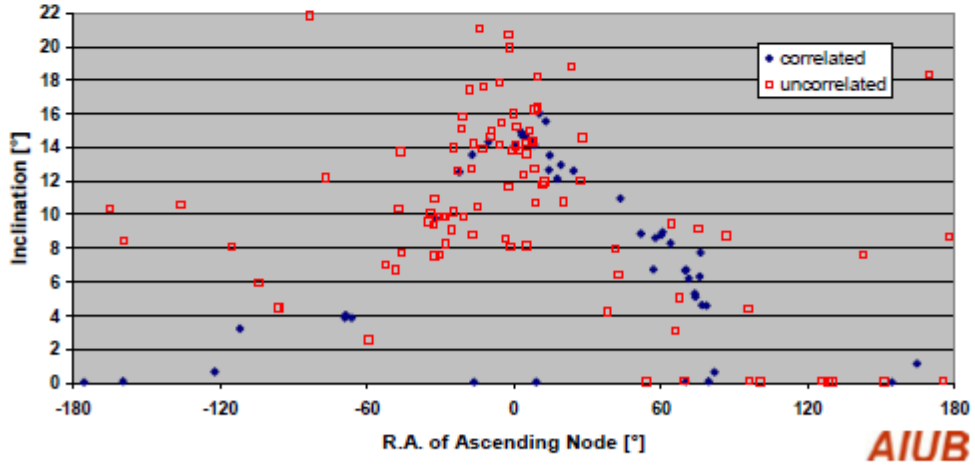

Figure 2-11: Inclination versus right ascension of ascending node for the detections from the IADC fields of the February to June 2008 sub-campaigns.

The correlated objects nicely show this evolutionary pattern. With a few exceptions the controlled satellites can be found at $i = 0°$ inclination at all right ascensions for their ascending nodes. But as the focus was on fields with higher inclinations, where we expected to detect more faint debris, there were only few controlled objects detected.

The bulk of the uncorrelated objects lies on the mentioned evolution track but with a much larger spread. In addition there is a 'background' component with a homogeneous distribution in the (Ω, i)-space noticeable in all six plots. The most striking features, however, are the distinct clusters of objects. Prominent concentrations are found in Figure 2-10 at $\Omega \approx 5°$, $i \approx 14°$, and $\Omega \approx -30°$, $i \approx 10°$.

We have checked some of the clusters for multiple sightings of one and the same objects and conclude that the clusters are real (a pure selection effect can thus be excluded). The only rational explanation for the origin of these clusters is breakup or collision events.

The explanation for the 'background' component is more difficult. A substantial part of this component may be an artifact due to the fact that both orbital elements are inferred from circular orbits. As explained in the paragraph on the distribution of the semimajor axes, objects on highly eccentric orbits like GTOs and high AMR GEO objects may affect the results and could at least partly be responsible for the 'background' component.

2.3.4 Conclusions

The results from the August 2003 to April 2008 campaigns confirm the results from earlier studies. The bimodal magnitude distribution is not only reflected in all yearly campaigns, but also in both types of surveys. Several clusters can be found in all campaigns. This is a further indication that the clusters are real. In addition, a precession of the cluster could be observed. Several indications were found that the GTO surveys are more sensitive to detect objects in GTO and in other highly eccentric orbits than the GEO surveys.

3 SUMMARY AND CONCLUSIONS

ESA supported the IADC AI 23.4 International 2007 Optical Debris Campaign In Higher Earth Orbit by acquiring optical survey observations from February 2008 to June 2008. All observations were acquired at the ESA 1-meter Space Debris Telescope (ESASDT) at the Teide Observatory at Tenerife, Canary Islands, Spain.

Observations were obtained during a total of 21 of the 37 internationally coordinated observation nights. The reason that ESA did not obtain data on 16 of the planned 37 nights was mostly unfavorable weather conditions.

ESA was combining the IADC search fields with fields of its ongoing survey campaigns in GEO and GTO, as well as with the necessary observations to maintain its catalogue of small-size debris.

The data presented in this report stems from 37 nights, including 21 nights where IADC survey field were observed. A total of 97.6 hours of survey observations were collected, 30 hours thereof were dedicated to IADC survey fields. The surveys resulted in 288 detections of un-

correlated and 163 detections of correlated objects. On the IADC fields only, 98 detections of uncorrelated and 48 detections of correlated objects were recorded.

The observations were highly successful and the results confirm and further improved the findings of the previous surveys like the IADC AI 21.2 International Space Debris Campaign in Higher Earth Orbit, revealing the existence of a substantial population of small-size debris in GEO, GTO and in other highly eccentric orbits. The GEO debris clouds in the orbital element space discovered in earlier studies could be confirmed.

A severe limitation of the surveys is given by the fact that circular orbits have to be inferred. Large inferred semimajor axes could, in particular, be caused by objects in GTO-like orbits or high AMR objects, which were observed near their apogee. The inferred orbital planes (inclination and node) are contaminated in a similar way by objects on non-circular orbits. In order to determine reliable 6-parameter orbits near-real-time follow-up observations of the detected objects would be required.

JAXA

Brief report of the observation at Nyukasa(JAXA innovative technology research center)

Toshifumi Yanagisawa(yanagisawa.toshifumi@jaxa.jp)

a. Description of the telescope and facilities used.
Telescope: Takahashi ε 350, D:355mm, f:1248mm(F/3.6)
Camera: N.I.L. CCD42-40, Chip:e2v CCD42-40
FOV: 1.27×1.27-degree

b. The obsevation method used.
No sidereal motion. The telescope changes its obsevational region every 5 minutes to follow the geocentric coordinates at the range of 42164km.

c. Data reduction methods.
Line-identifying technique developed by JAXA was used. The line-identifying technique needs 18 consecutive CCD frames with 3-second exposure time. First, it detects candidate objects using a threshold and a shape parameter. Then, it finds any series of objects that are arrayed on a straight line from the first frame to the last frame. In this analysis, 400 candidates of each frame were used to find objects.

d. Calibration techniques.
In order to determine the coordinates of detected objects, the matching algorithm of IRAF (ccxymatch, ccmap and cctran) and the guide star catalog ver 1.1 were used. The guide star catalog ver 1.1 was also used to estimate the magnitude of detected objects.

e. Summary
This could include histograms of magnitude, inclination, and semi-major axis of detected CT and UCT. This could also include distribution of CT and UCT in the RAAN-inclination plot.

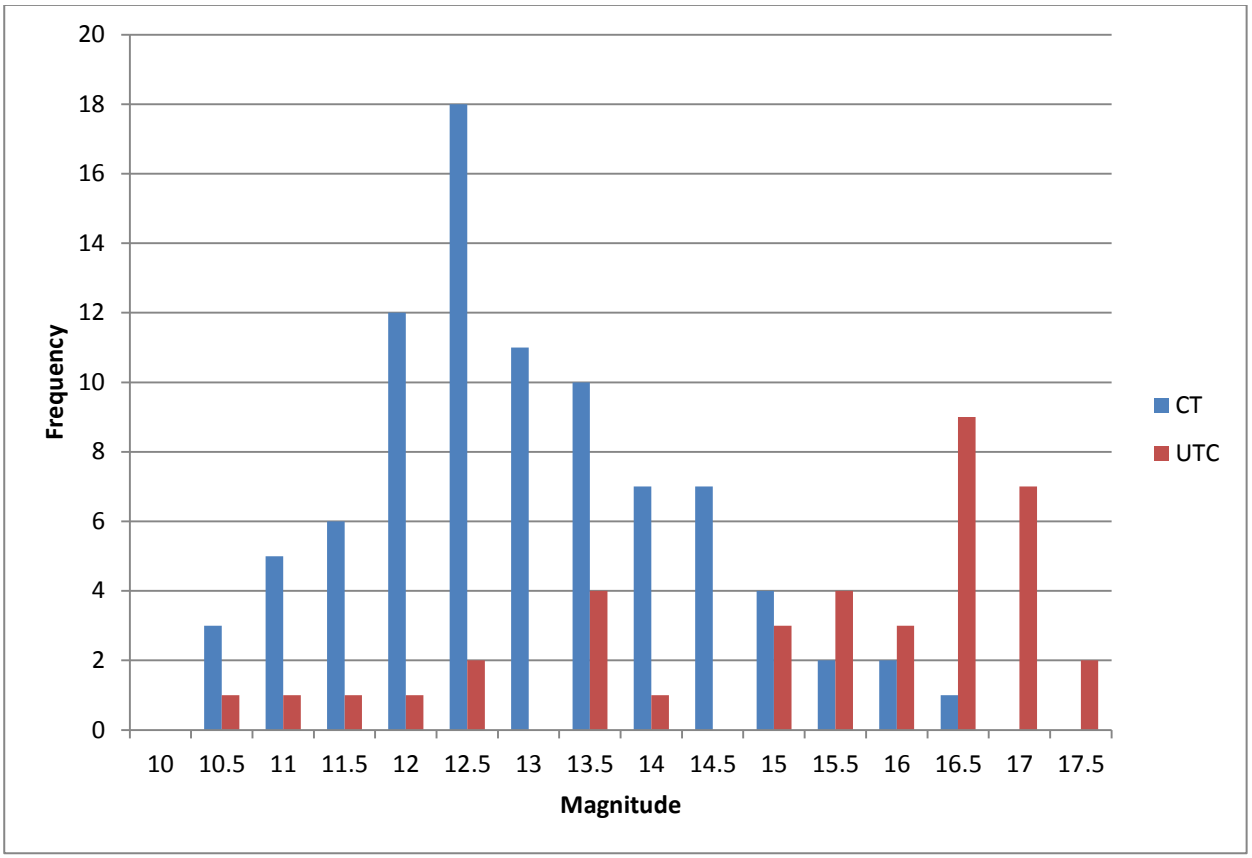
20
18
16
14
12
10
8
6
4
2
0
Frequency
10
10.5
11
11.5
12
12.5
13
13.5
14
14.5
15
15.5
16
16.5
17
17.5
Magnitude
CT
UTC

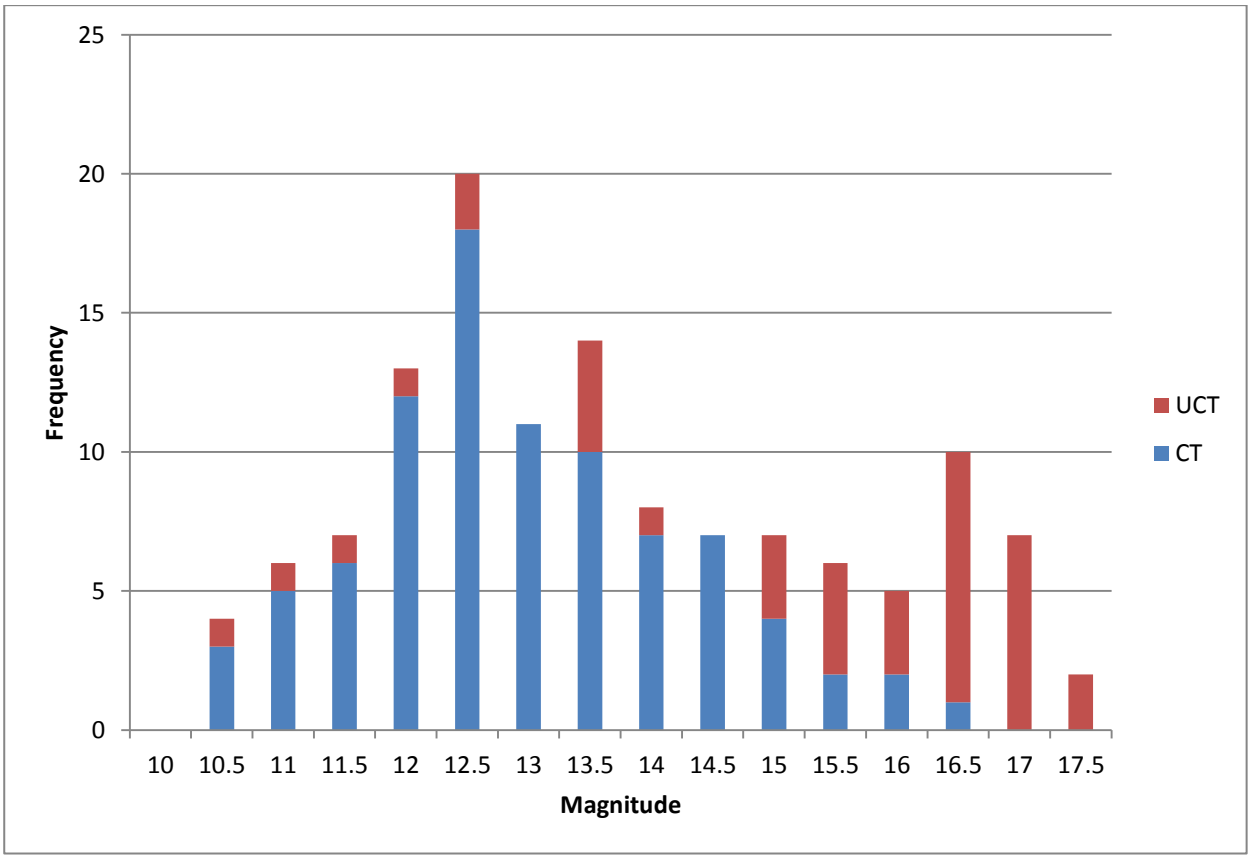
25
20
15
10
5
0
Frequency
10
10.5
11
11.5
12
12.5
13
13.5
14
14.5
15
15.5
16
16.5
17
17.5
Magnitude
UCT
CT

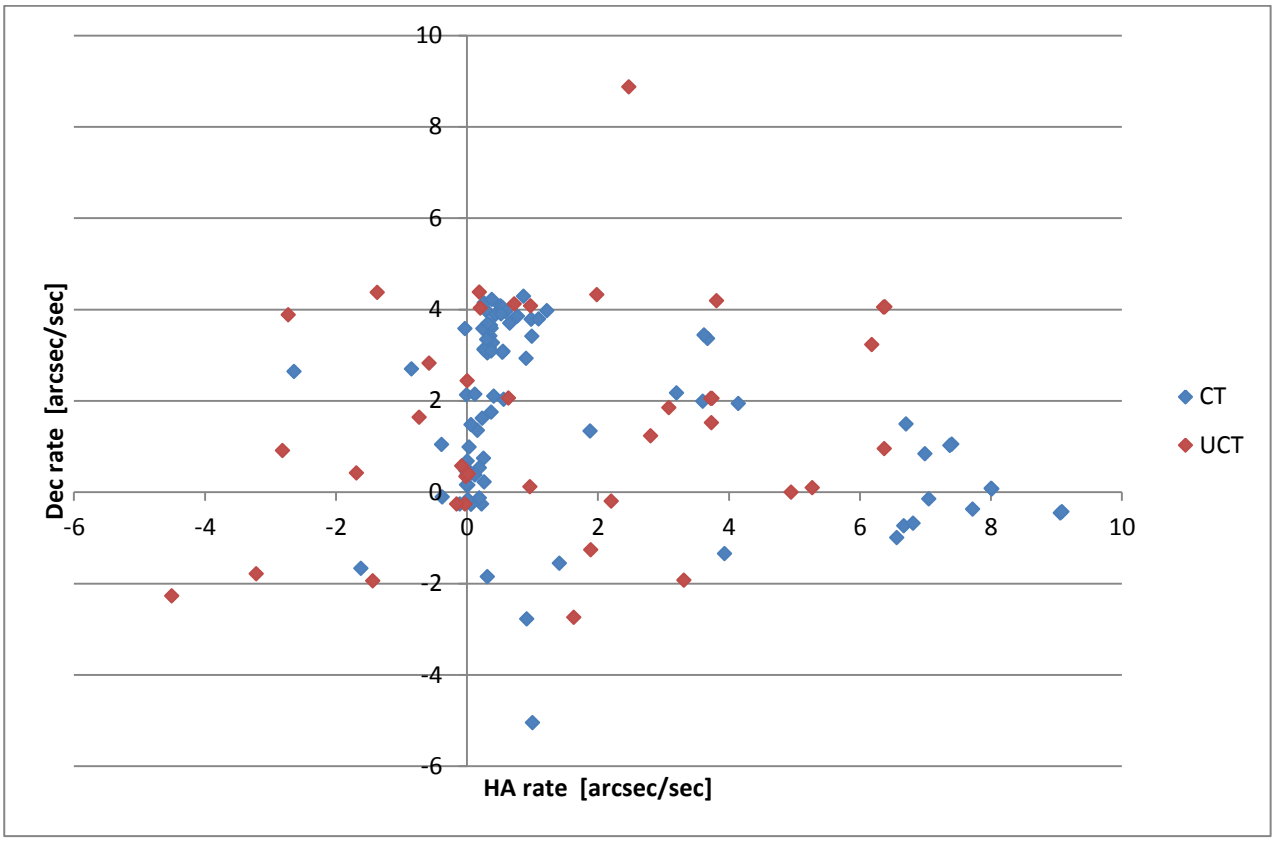
10
8
6
4
2
0
-2
-4
-6
-6
-4
-2
0
2
4
6
8
10
Dec rate [arcsec/sec]
HA rate [arcsec/sec]
CT
UCT

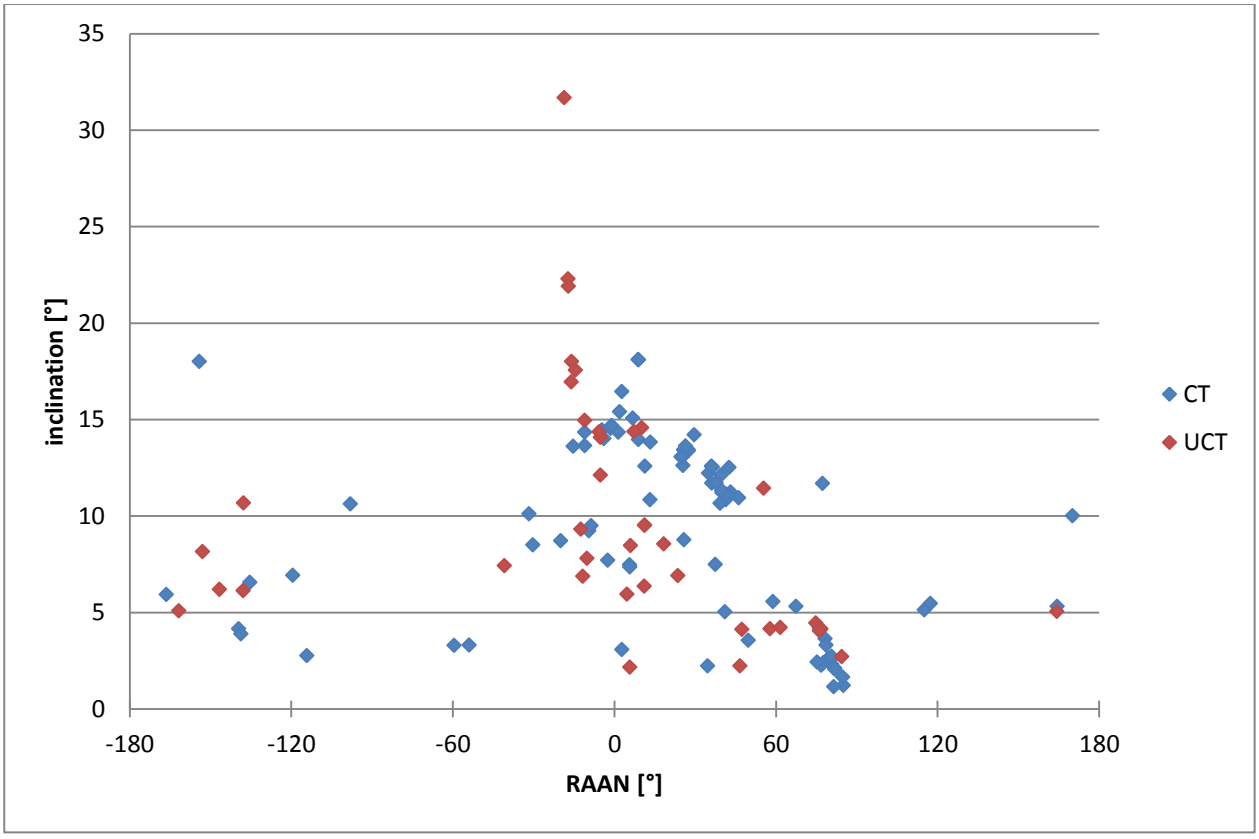
35
30
25
20
15
10
5
0
-180
-120
-60
0
60
120
180
inclination [°]
RAAN [°]
CT
UCT

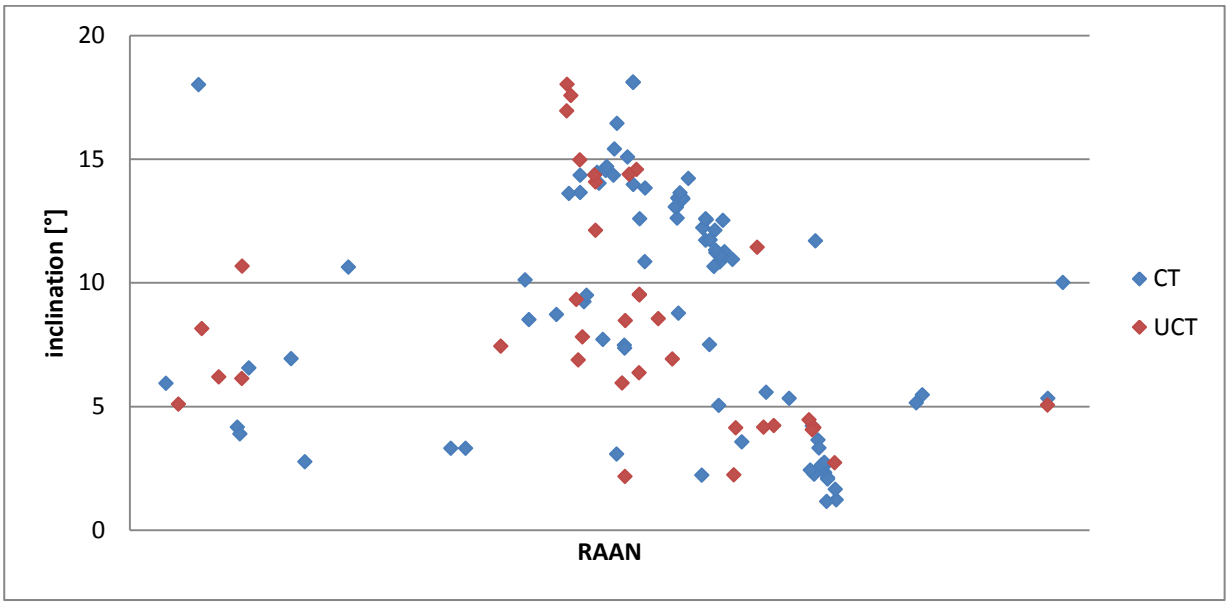
20
15
10
5
0
inclination [°]
RAAN
CT
UCT

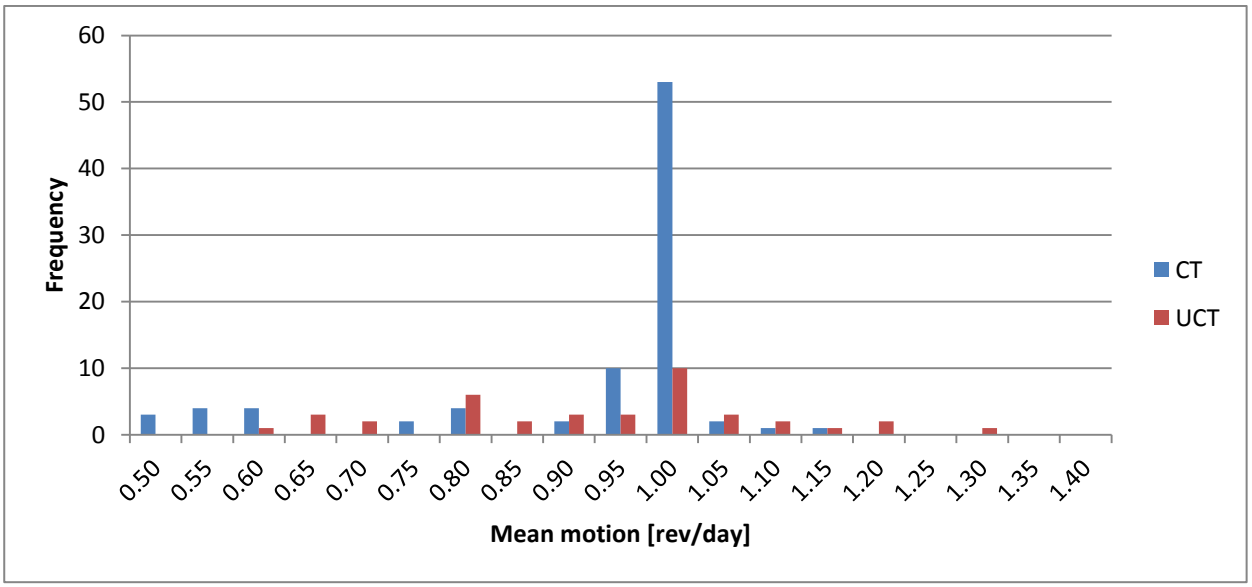
60
50
40
30
20
10
0
Frequency
0.50
0.55
0.60
0.65
0.70
0.75
0.80
0.85
0.90
0.95
1.00
1.05
1.10
1.15
1.20
1.25
1.30
1.35
1.40
Mean motion [rev/day]
CT
UCT

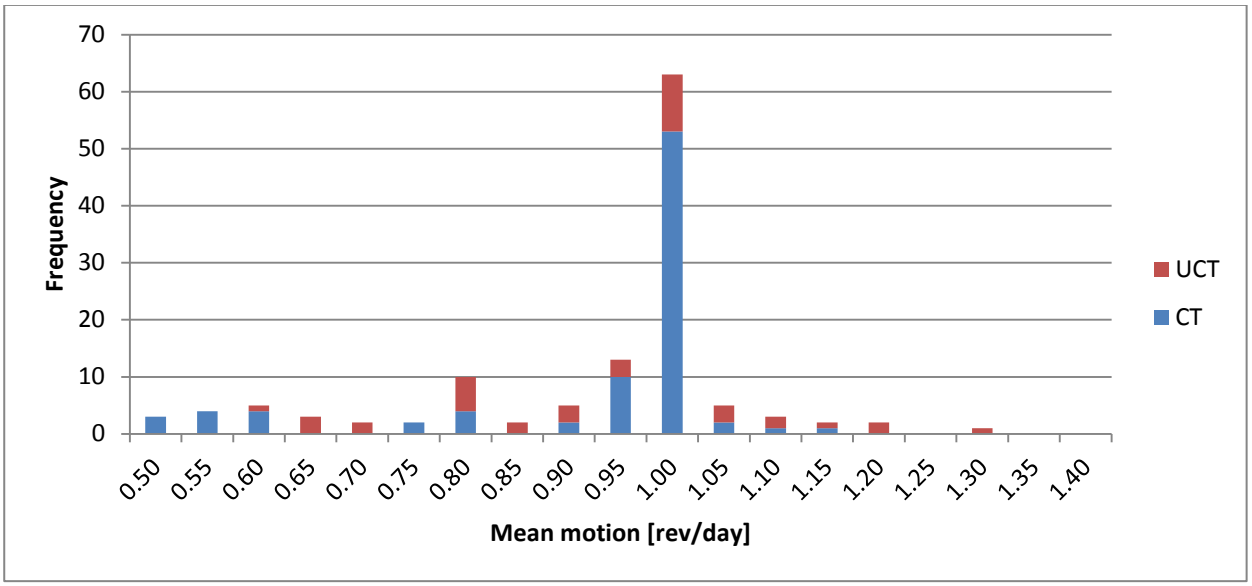
70
60
50
40
30
20
10
0
Frequency
0.50
0.55
0.60
0.65
0.70
0.75
0.80
0.85
0.90
0.95
1.00
1.05
1.10
1.15
1.20
1.25
1.30
1.35
1.40
Mean motion [rev/day]
UCT
CT

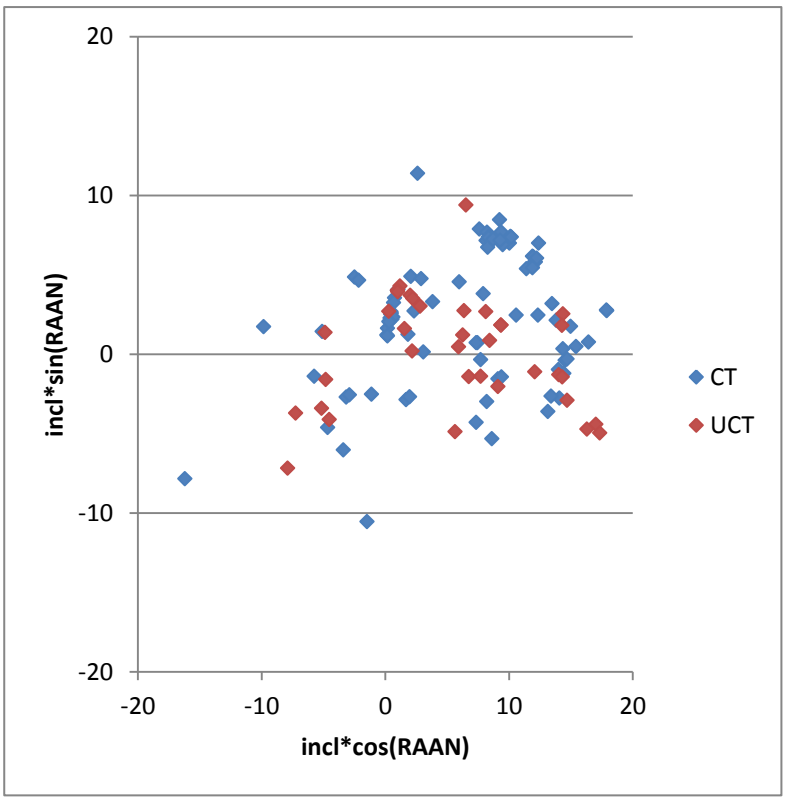
20
10
0
-10
-20
incl*sin(RAAN)
-20
-10
0
10
20
incl*cos(RAAN)
CT
UCT

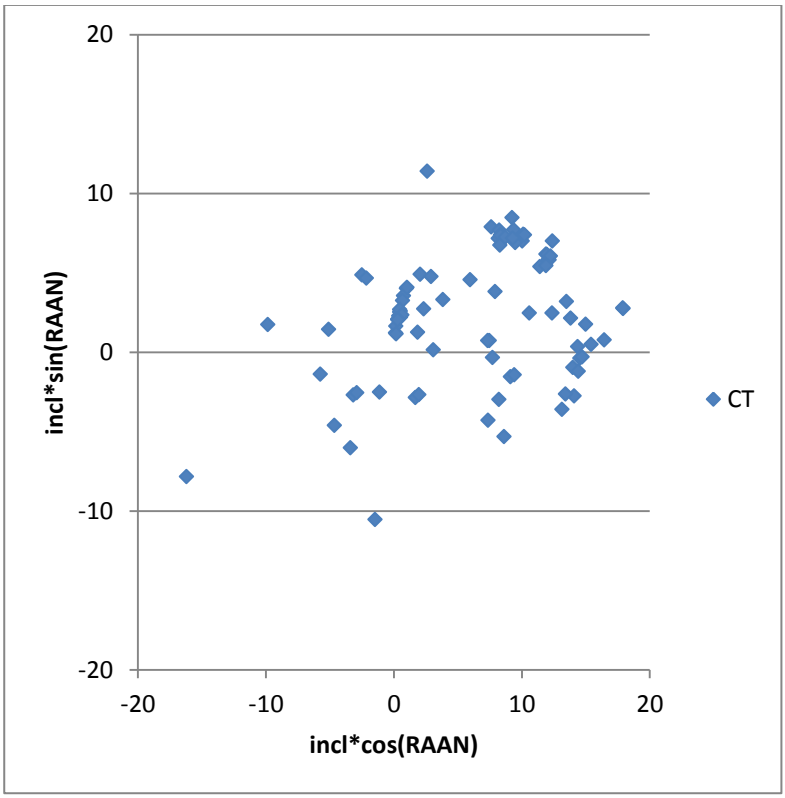
20
10
0
-10
-20
-20
-10
0
10
20
incl*sin(RAAN)
incl*cos(RAAN)
CT

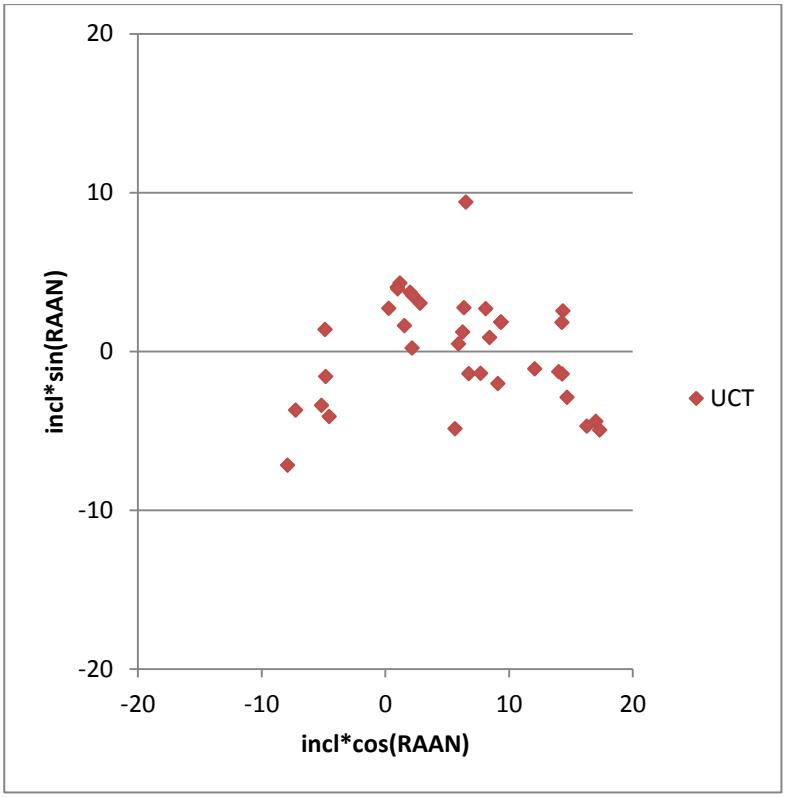
20
10
0
-10
-20
-20
-10
0
10
20
incl*sin(RAAN)
incl*cos(RAAN)
UCT

NASA

NASA OPTICAL OBSERVATIONS OF GEO SPACE DEBRIS: A REPORT TO THE IADC FOR AI23.4

Patrick Seitzer
University of Michigan, Dept. of Astronomy, 818 Dennison Bldg, Ann Arbor, MI 48109-1042, USA
Email: pseitzer@umich.edu

Kira Abercromby
Aerospace Engineering Department
California Polytechnic State University
San Luis Obispo, USA

Heather Cowardin
ESCG/Jacobs Sverdrup, Houston TX 77058, USA

Edwin Barker
LZ Technology, Houston TX 77058, USA

1. INTRODUCTION

This document summarizes observations and results obtained from January through September 2007 of space debris at geosynchronous Earth orbit (GEO) in support of an international observing campaign organized by the Inter-Agency Space Debris Coordination Committee (IADC). The purpose of the campaign was to measure the population of space debris at GEO, and determine the distributions in brightness and derived orbital parameters.

All of the work reported here was supported by NASA's Orbital Debris Program Office, Johnson Space Center, Houston, Texas.

2. DESCRIPTION OF OBSERVATIONAL TECHNIQUES

All data were obtained with the University of Michigan's Curtis-Schmidt telescope located at the Cerro Tololo Inter-American Observatory in Chile (longitude = 70.8 degrees West, latitude = 30.2 degrees South, altitude = 2216 meters). From this location one can observe orbital longitudes ranging from 25 degrees west to 135 degrees west, which covers most of the orbital slots assigned to the continental US.

The telescope is a 0.61/0.91-m f/3.5 Schmidt of classical design. A 2048x2048 SITe thinned, backside illuminated CCD is mounted at Newtonian focus. The field of view is 1.3x1.3 degrees, with 2.318 arc-second pixels. All images are obtained through a broad R filter (200 nm FWHM) selected to maximize detected counts from objects with a reflected solar spectrum, and yet at the same time minimize signal from night sky emission lines and the effects of atmospheric refraction. Standard exposure time is 5 seconds, which reaches a signal-to-noise (S/N) of 10 for an 18^{th} magnitude object. All magnitudes are referred to the Cousins R system of astronomical magnitudes, and calibrated by nightly observations of Landolt standard stars.

In order to maximize the apparent brightness of GEO objects, all observations are taken as close as possible to the anti-solar point but just outside of eclipse. The telescope tracks a point of constant right ascension and declination at the sidereal rate. During the exposure, the charge on the CCD is shifted in the reverse direction of diurnal motion so that objects at GEO appear as point sources or as short streaks. To first order the telescope tracks the anti-solar

point while the detector tracks the object. The observed brightness of any object at GEO is maximized by staying close to the anti-solar point while at the same time minimizing streak losses.

Each clear night, the system takes a 5 second exposure every 37.9 seconds. A strip of sky 1.3 degrees high by over 100 degrees long is covered. The next night the telescope is offset in declination, and another strip of sky is scanned. Typically over 700 images are obtained each night.

The CCD frames are processed in real-time: including instrumental signature removal (bias subtraction and flat fielded), and processed through an object finder that detects point sources and short streaks.

During the 5.3 minutes that it takes a GEO object to drift across the field of view, 8 independent detections of each source are made. At this time, a fairly conservative limit has been set to minimize the chance of false detections. 4 independent detections are required for a source to be considered real. This sets the detection limit to be just fainter of R = 18, corresponding to a signal to noise (S/N) of 10 for an individual measurement.

Each detection yields a measurement of the source's brightness and position. Correlating detections from frame to frame yields the observed angular motion over an average time span of 5.3 minutes. At this time we are looking for sources that are moving slowly with respect to station-keeping objects, and so the angular rate box that is searched is limited to ± 2 arc-seconds/second in hour angle, and ± 5 arc-seconds/second in declination. This angular rate box size was determined from analysis of NASA's CDT (CCD Debris Telescope) observations of brighter debris at GEO, and will comfortably cover the expected range of angular motions for objects released at zero velocity from a geostationary position, and then subject to the three dominant perturbations of the Sun, Moon, and Earth's bulge.

All correlations are manually verified to guard against false positives in the automatics object detection and correlation pipeline.

Positions, magnitudes, and times of all verified detections are sent each morning after observing to NASA's Orbital Debris Program Office at the Johnson Space Center in Houston, Texas, for further analysis.

Operated in this manner for GEO debris observations, the system is given the acronym **MODEST**, for **M**ichigan **O**rbital **DE**bris Survey **T**elescope.

2. OBSERVATIONAL RESULTS

The IADC campaign was scheduled for 14 nights in two 7 night runs centered on new moon during Feb and March 2008, the best time of the year for observing from Chile. Data was obtained on all 14 nights. A total of 8943 images were obtained and analyzed.

Figure 1 shows the observed Cousins R magnitude diagram for all objects which have 4 or more detections. No attempt has been made to remove duplicates, where the same objects appeared in the data set on multiple nights. The term corrected magnitude means that the observed, calibrated magnitudes from MODEST have been corrected to a solar phase angle of zero degrees, and to a standard GEO distance of 36,000 km.

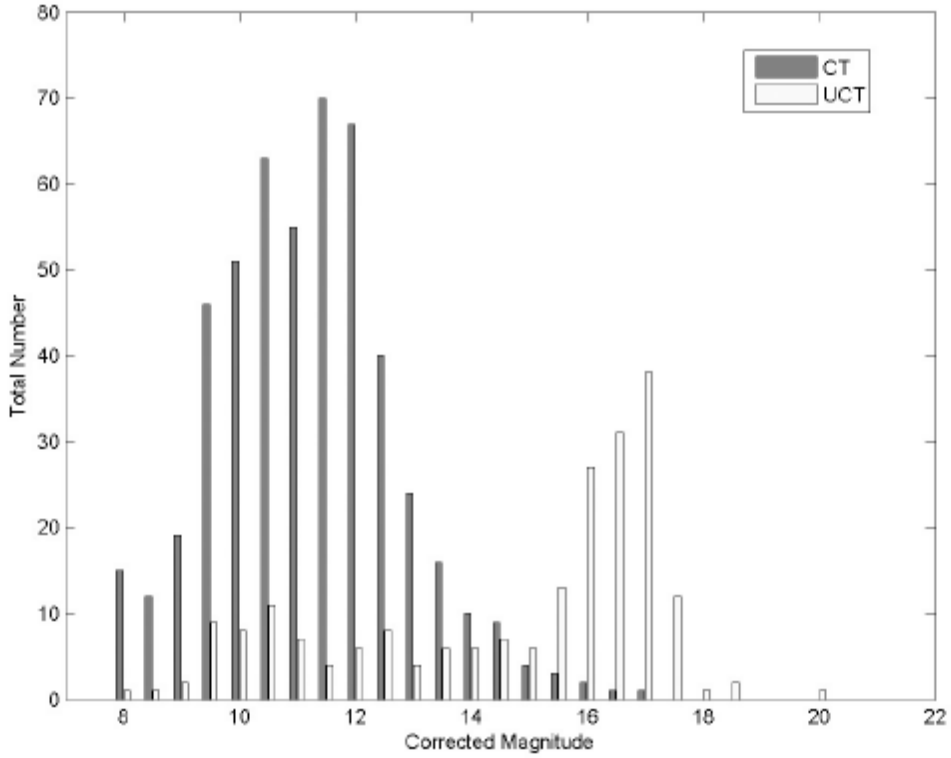

Figure 1. Histogram of observed magnitudes for all objects detected in all four observing runs (January through September 2004). CT refers to correlated targets (in the public catalog), while UCT refers to observed objects which are not in the catalog.

The peak at the bright end (near R = 11.5) is dominated by bright intact spacecraft.

The correlation between a MODEST object and the public US satellite catalog was done at the Orbital Debris Program Office at the Johnson Space Center. CT refers to an object which is in the public catalog, UCT refers to an object which is not. Not surprisingly, the MODEST observations go fainter than the public catalog.

The cutoff at R = 18th magnitude is not a true cutoff in the real distribution of debris, but rather due to selection effects in the observing system.

For conversion between our R magnitudes, and a Johnson V magnitude, we use a value for solar V-R = 0.363 (Stritzinger et al., 2005 PASP 117:810-822). Objects will be fainter in V by 0.363 magnitudes if they have a neutral color reflecting a solar spectrum.

This figure shows the same qualitative distribution as seen in prior IADC campaigns by MODEST: a peak near 12th magnitude of intact spacecraft and rocket bodies, and a fainter peak near 17th magnitude of smaller debris pieces. As stated above, the falloff in numbers fainter than 17th magnitude is due to system sensitivity limits and should not be interpreted as a real falloff.

3. ORBITAL PARAMETERS

Positions, magnitudes, and times of all objects with four or more detections are sent to NASA's Orbital Debris Program Office at the Johnson Space Center in Houston, Texas, where orbits are computed.

For orbit determinations, the orbit is assumed to be circular (zero eccentricity). This assumption is made because a 5.3 minute arc length in an orbit with a period = 23h56m is not long enough to solve for all orbital elements with any degree of reliability. Figure 2 shows the plot of right-ascension of the ascending node (RAAN) versus inclination for all objects in the sample. Different symbols are used for CT and UCT. Again, no effort has been to remove objects which may appear on different nights.

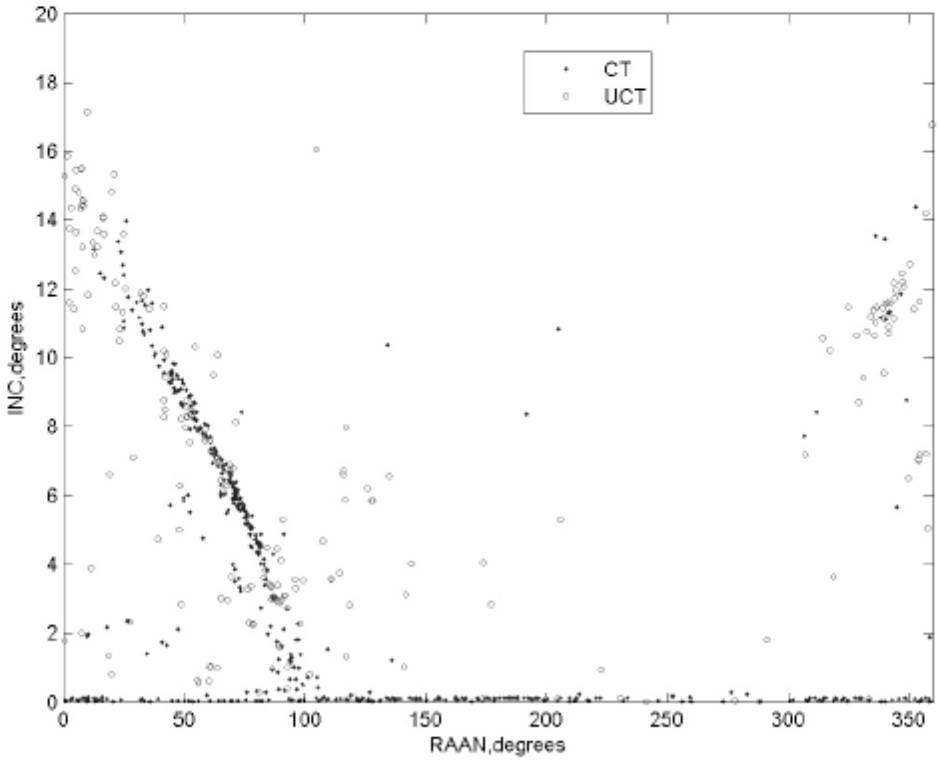

Figure 2. Plot of inferred RAAN (right-ascension of the ascending node) versus inferred inclination for all objects in the MODEST sample.

The CTs at inclination very near 0.0 are station-keeping objects, while the well defined line of CTs on the left hand side of the plot follow a locus predicted by gravitational perturbations of the Sun, Moon, and Earth's bulge acting over time on an object released at zero velocity from a pure geostationary point. The UCTs, however, are more broadly distributed in the RAAN-inclination plane.

Figure 3 (below) shows the distribution of inclinations for all objects in the MODEST sample. This is dominated by station-keeping objects with orbital inclination near zero.

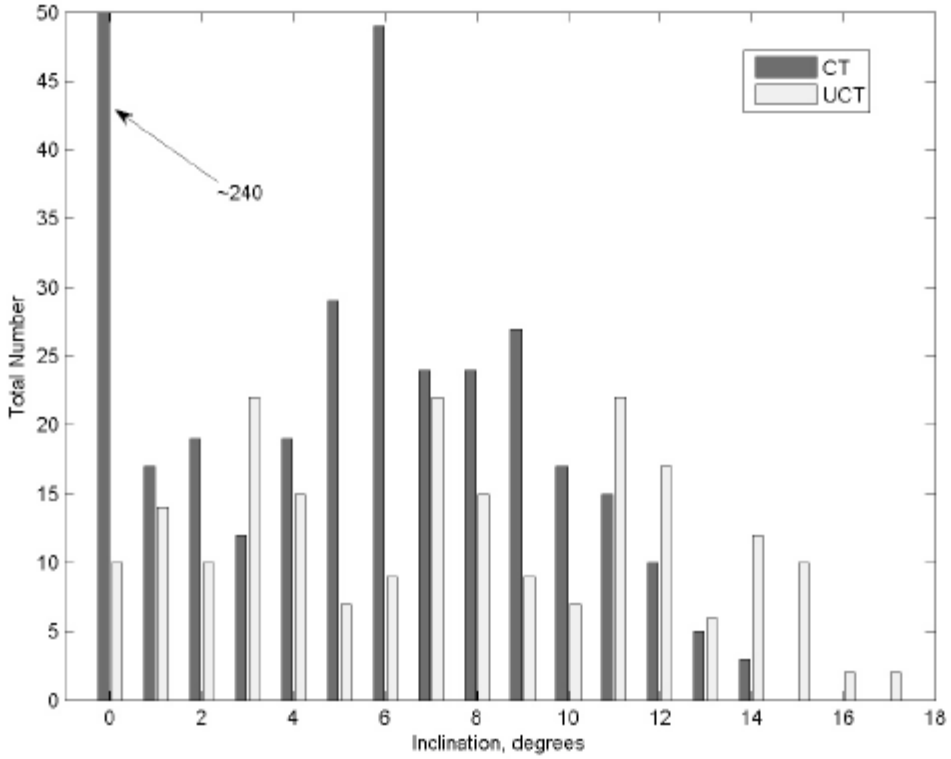

Figure 3. Histogram of the orbital inclination for all objects. The distribution is dominated by objects from the four nights when the station-keeping belt (latitude = 0 degrees) was scanned.

Finally, figure 4 (below) shows the classic polar plot of all objects in the MODEST sample.

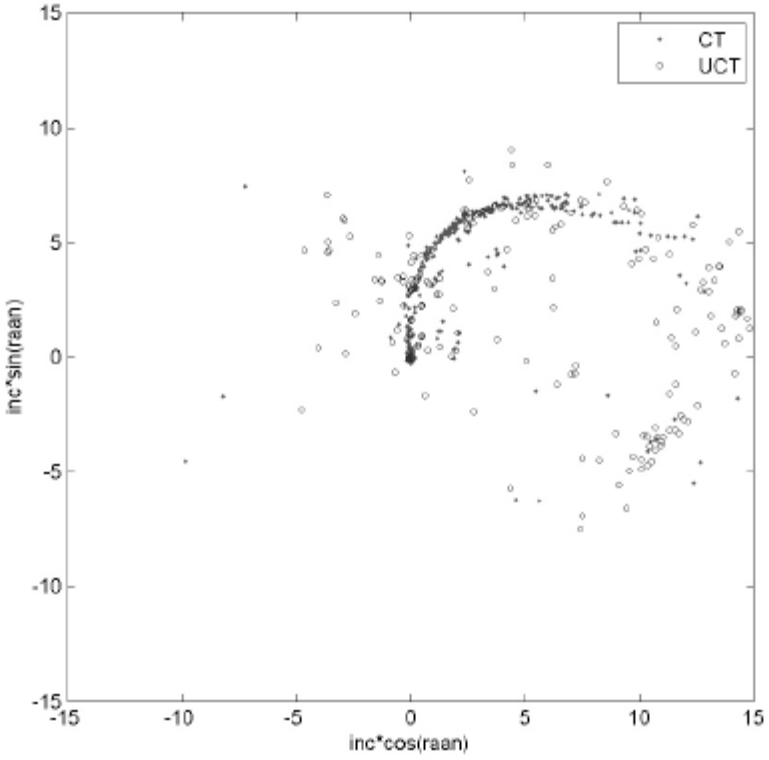

Figure 4. Standard polar plot of all detections in the MODEST sample. Bright CT's tend along the locus of points, while UCTs (which tend to be fainter) have a broader distribution.

4. COVERAGE IN RAAN-INC PLANE

By modeling the time and direction of the actual observations, along with the orbits that would be seen at that time and in that direction, a quantitative measure of how much of the total phase space of orbits sampled during the observing campaign can be produced. Because we assume circular orbits in order to derive orbital parameters, we limit our analysis to the plane defined by RAAN (Right Ascension of Ascending Node) and INC (inclination). This is shown in figure 5 below.

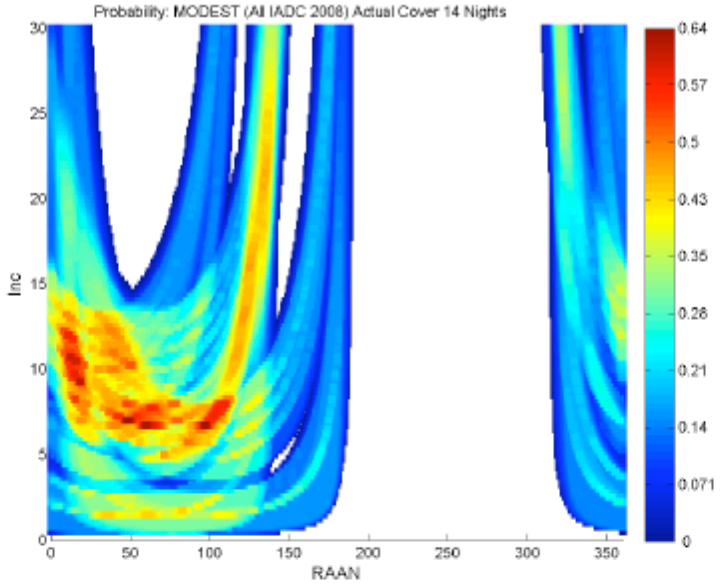

Figure 5. Sensitivity of observations to location in the RAAN-INC plane.

With only two observing runs at the same time of year, it is impossible to cover the entire RAAN-INC plane. The gap in the 200 to 300 degrees of RAAN could be filled in by observing at a different time of year. The particular RA-DEC observing positions selected for each night in February and March 2008 resulted in heavy emphasis on orbits of objects released at zero velocity at GEO, and then perturbed up to the maximum inclination of 15 degrees.

A similar analysis was done for sampling in the XY plane (see figure 4 above), and is shown in Figure 6 below.

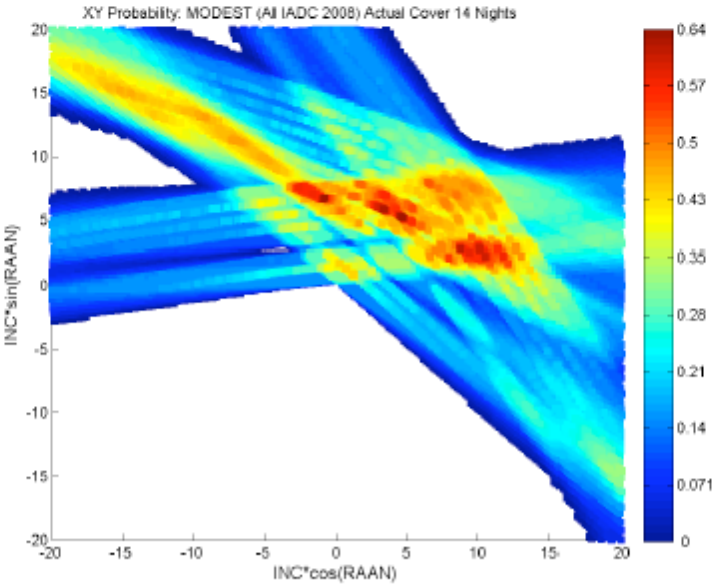

Figure 5. Sensitivity of observations in the classic polar plot.

What these plots show is the tremendous variation in the sampling efficiency is different regions of the total orbital phase space. This complicates any attempt to derive the total GEO population from observations taken over a small time frame and over a limted area of sky.

5. ACKNOWLEDGEMENTS

P. Seitzer thanks NASA's Orbital Debris Program Office for generous support to the University of Michigan for this project. The authors are very grateful to the Director and staff of the Cerro Tololo Inter-American Observatory for their encouragement and mountain top support during all aspects of observing.

UKSA

For Working Group 1 Action Item AI 23.4 (International 2007 Optical Debris Campaign In Higher Earth Orbit) the UK delegation had no large-aperture sensor available with which to make faint or small object debris surveys. The optical sensors available for participation in the campaign were the Starbrook sensors which are not suited to surveys for small debris because their detection limit at the GEO orbit is ~ 1 m^2.

However, the large field of view and high level of automation of the Starbrook sensors make them well suited to test and demonstrate survey methods and operational procedures. Analysis of these methods and procedures may then be taken into consideration for planning future surveys.

AI 23.4 deliberately included all higher Earth orbits rather than just the geosynchronous orbits sampled in previous optical observing campaigns. The wording was designed to encourage sharing between members of the working group of observing experiences in diverse orbital regimes. The UK delegation therefore decided to use the large field of view sensors available to it to carry out a trial survey-and-chase of a MEO region. As far as has been reported through IADC WG1, few MEO surveys have previously been undertaken, not least because of the large size of the orbit space that needs to be sampled. However the large fields of view of the UK's Starbrook sensors seemed well suited to such a task.

Furthermore, the highly automated nature of the Starbrook sensors means that it is possible to use the co-located companion sensor for immediate follow-up of any unidentified objects to obtain an improved orbit, including an estimate of eccentricity. Thus follow-up observations can be acquired without breaking the survey pattern so ensuring a leak-proof survey fence.

A full discussion of the results of the MEO survey and follow-up observations was given in a paper to the 5th ESA Space Debris Conference in Darmstadt in 2009 so only a brief outline is recorded here. Those interested in a fuller account should consult the conference proceedings; a pre-print is available at http://www.spaceinsight.co.uk.

The Starbrook sensor used for the MEO survey had a field of view of 10° x 6° and an aperture of 100 mm. This sensor could maintain a leak-proof fence 20° wide at ascending (or descending) node. To improve the signal to noise of any MEO object crossing its field of view the sensor used open-loop tracking in declination to capture objects ascending or descending through the fence; the typical motion of a MEO object at node crossing is, for a sensor static in hour angle, almost entirely in the declination axis.

If an object was encountered that could not be correlated then the survey sensor was able to cue its companion sensor (which had greater sensitivity but a smaller 4°x4° field of view).

The two sensors carried out the survey for a total of 18 nights spread over two new Moon periods. The nights were mixed between 20° ascending, 20° descending, and 10° ascending and descending node fences (achieved by choice of open-loop tracking direction).

After careful analysis no debris was detected during either of the survey periods.

The unknown object follow-up by the companion sensor was triggered on a number of occasions and operated successfully in obtaining orbits with sufficient precision that the objects could be re-acquired on the next night. Analysis showed that all the unknown objects were observations of a newly launched Glonass satellite which was still being manoeuvred into its working orbit, so the orbital elements used for identification were not up to date.

The lack of debris from the surveys meant that the UK delegation did not enter any results into the campaign. The 1 m^2 detection limit of the survey sensor means that any debris found would have been large enough that it is unlikely they would have eluded serendipitous observation during target-by-target tracking of the MEO population. Since the survey only sampled ~ 0.2% of the $\{\Omega, m, i\}$ orbit space the null result is not deemed to be statistically significant.